Atmos. Chem. Phys. Discuss., 14, 2883–2934, 2014
www.atmos-chem-phys-discuss.net/14/2883/2014/
doi:10.5194/acpd-14-2883-2014

Atmospheric Chemistry and Physics Discussions

Long-term MAX-DOAS network observations of NO_2 in Russia and Asia (MADRAS) during 2007–2012: instrumentation, elucidation of climatology, and comparisons with OMI satellite observations and global model simulations

Y. Kanaya[1], H. Irie[1,a], H. Takashima[1,b], H. Iwabuchi[1,c], H. Akimoto[1,d], K. Sudo[2], M. Gu[3], J. Chong[3], Y. J. Kim[3], H. Lee[3,e], A. Li[4], F. Si[4], J. Xu[4], P.-H. Xie[4], W.-Q. Liu[4], A. Dzhola[5], O. Postylyakov[5], V. Ivanov[5,f], E. Grechko[5], S. Terpugova[6], and M. Panchenko[6]

[1]Research Institute for Global Change, Japan Agency for Marine-Earth Science and Technology, Yokohama 2360001, Japan
[2]Nagoya University, Nagoya 4648601, Japan

[3]Gwangju Institute of Science and Technology (GIST), Gwangju 500712, Korea
[4]Anhui Institute of Optics and Fine Mechanics, Chinese Academy of Sciences, Hefei 230031, China
[5]A. M. Obukhov Institute of Atmospheric Physics, Russian Academy of Sciences, Moscow 119017, Russia
[6]V. E. Zuev Institute of Atmospheric Optics, Siberian Branch of the Russian Academy of Sciences, Tomsk 634021, Russia
[a]now at: Chiba University, Chiba 2638522, Japan
[b]now at: Fukuoka University, Fukuoka 8140180, Japan
[c]now at: Tohoku University, Sendai 9808578, Japan
[d]now at: Asia Center for Air Pollution Research, Niigata 9502144, Japan
[e]now at: Pukyong National University, Pusan 608737, Korea
[f]now at: National Ozone Monitoring Research and Educational Center of Belarusian State University (NOMREC BSU), Minsk 220064, Belarus

Received: 29 November 2013 – Accepted: 15 January 2014 – Published: 28 January 2014

Correspondence to: Y. Kanaya (yugo@jamstec.go.jp)

Published by Copernicus Publications on behalf of the European Geosciences Union.

ACPD
14, 2883–2934, 2014

Abstract

We conducted long-term network observations using standardized Multi-Axis Differential optical absorption spectroscopy (MAX-DOAS) instruments in Russia and ASia (MADRAS) from 2007 onwards. At seven locations (Cape Hedo, Fukue, and Yokosuka in Japan, Hefei in China, Gwangju in Korea, and Tomsk and Zvenigorod in Russia) with different levels of pollution, we obtained 80 927 retrievals of tropospheric NO_2 vertical column density (TropoNO2VCD) and aerosol optical depth (AOD). In the technique, the optimal estimation of the TropoNO2VCD and its profile was performed using aerosol information derived from O_4 absorbances simultaneously observed at 460–490 nm. This large data set was used to analyze NO_2 climatology systematically, including temporal variations from the seasonal to the diurnal scale. The results were compared with Ozone Monitoring Instrument (OMI) satellite observations and global model simulations. Two NO_2 retrievals of OMI satellite data (NASA ver. 2.1 and Dutch OMI NO_2 (DOMINO) ver. 2.0) generally showed close correlations with those derived from MAX-DOAS observations, but had low biases of ~ 50 %. The bias was distinct when NO_2 was abundantly present near the surface and when the AOD was high, suggesting that the aerosol shielding effect could be important, especially for clean sites where the difference could not be attributed to the spatial inhomogeneity. Except for constant biases, the satellite observations showed nearly perfect seasonal agreement with MAX-DOAS observations, suggesting that the analysis of seasonal features of the satellite data were robust. The prevailing seasonal patterns with a wintertime maximum implied the dominance of anthropogenic emissions around our sites. The presence of weekend reductions at Yokosuka and Gwangju suggested the dominance of emissions from diesel vehicles, with significant weekly cycles, whereas the absence of such a reduction at Hefei suggested the importance of other sources. A global chemical transport model, MIROC-ESM-CHEM, was validated for the first time with respect to background NO_2 column densities during summer at Cape Hedo and Fukue in the clean marine atmosphere.

ACPD
14, 2883–2934, 2014

1 Introduction

Nitrogen oxides (NO_x), i.e., NO and NO_2, are key chemical species in driving tropospheric photochemistry, and they participate in the mechanisms used to explain local to global air pollution. They are originally emitted or produced from natural (soil and lightning) and anthropogenic sources, and are strongly involved in the chain reactions forming tropospheric ozone (O_3). The reaction of NO with peroxy radicals (HO_2 and organic peroxy radicals, RO_2) produces NO_2, resulting in net production of O_3 via subsequent photolysis of NO_2. This reaction simultaneously recycles OH radicals, which determine the atmospheric oxidative capacity, and this sustains the concentration levels of peroxy radicals. Under heavily polluted conditions, NO_2 provides a major pathway for loss of OH, nonlinearly controlling the oxidative capacity. The deposition of nitric acid, produced from the reaction of OH + NO_2, and of nitrate aerosols, normally formed by gas-to-particle partition of nitric acid, on the Earth's surface fertilizes terrestrial and marine ecosystems (Duce et al., 2008), as well as causing acidification. Knowledge of global and regional distributions of NO_2, their temporal variations, and the underlying mechanisms therefore provides a firm basis for investigations of multi-scale air pollution and the nitrogen cycle.

Recent orbiting satellite sensors have enabled monitoring of the tropospheric NO_2 vertical column density (TropoNO2VCD) from the regional to the global scale (e.g., Burrows et al., 1999). Past studies have shown that large spatial inhomogeneity, strong seasonal variations, and long-term trends are present (e.g., Richter et al., 2005; Boesma et al., 2007; Martin et al., 2006; van der A et al., 2008). In Asia, particularly Central East China (110–122° E, 30–40° N), the highest TropoNO2VCD values in the world have been recorded in recent years. Compared with the aerosol optical depth (AOD), another observable parameter from satellite sensors, for which various types of ground-based long-term monitoring networks such as AERONET (AErosol RObotic NETwork, Holben et al., 2001), SKYNET (http://atmos.cr.chiba-u.ac.jp/), and light detection and ranging (lidar) networks can provide a firm basis for validation, Tro-

ACPD
14, 2883–2934, 2014

poNO2VCD has been evaluated with independent observations relatively infrequently. It is strategically important to certify satellite observations through comparisons with qualified observations regarded as ground truth; the verified spatial distributions or temporal variations are then used for further analysis.

In the past, aircraft-based in situ observations (Bucsela et al., 2008; Celarier et al., 2008), ground-based direct-sun Brewer measurements (Wenig et al., 2008), zenith DOAS (differential optical absorption spectroscopy) (Chen et al., 2009), lidar systems (Hains et al., 2010), urban air quality monitoring networks (Boersma et al., 2008), and combinations with model simulations (Lamsal et al., 2010) have been used for validation of satellite-based observations of tropospheric NO_2. Multi-axis DOAS (MAX-DOAS) observations (Hönninger et al., 2004; Wittrock et al., 2004; Sinreich et al., 2005) have also been proven to provide suitable columnar data for validation of satellite observations. In the past, MAX-DOAS observations over relatively short periods have been used for the validation of satellite-based observations of tropospheric NO_2 (e.g., Heue et al., 2005; Brinksma et al., 2008; Celarier et al., 2008; Irie et al., 2008a, 2009a; Hains et al., 2010; Shaiganfar et al., 2011; Peters et al., 2012). For more systematic validation, a long-term ground-based monitoring network for NO_2 is highly desirable.

So far, several MAX-DOAS network observations have been reported. Two of these, established at an early stage, are the BREDOM (Bremian DOAS network for atmospheric measurements) network, including Bremen, Ny-Ålesund, Nairobi, Mérida, and Heraklion (e.g., Wittrock et al., 2004), and a network maintained by the Belgian Institute for Space Aeronomy (BIRA-IASB) (http://uv-vis.aeronomie.be/groundbased/), including Harestua, Jungfraujoch, Observatoire de Haute-Provence (OHP), Reunion Island, Beijing, and Uccle (e.g., Clémer et al., 2010). At these sites, high-quality spectroscopy is performed using high-grade spectrometers and charged-couple device (CCD) detectors, enabling retrievals of weak absorbers (e.g., BrO) in the troposphere and stratosphere. Valks et al. (2011) used MAX-DOAS observations of TropoNO2VCD at OHP for 4 yr to validate Global Ozone Monitoring Experiment-2 (GOME-2) satellite obser-

ACPD
14, 2883–2934, 2014

vations. Hendrick et al. (2013) studied temporal variations in NO_2 and HONO derived from MAX-DOAS observations for 4 yr in and near Beijing.

As a Global Earth Observation System of Systems (GEOSS)-related project funded by the Japanese government during FY2006–2010, we established a long-term NO_2-monitoring network based on MAX-DOAS over Russia and Asia (MADRAS). This paper provides an overview of these network observations. Our strategy is to use a relatively low-cost miniature spectrometer to obtain spectra of compromised, but still sufficient, quality. A similar approach was used for a network for monitoring volcano plumes (Galle et al., 2010). Recently, the Max Planck Institute reported long-term observations of NO_2 in Beijing using a low-cost MAX-DOAS instrument and comparisons of the data with satellite observations (e.g., Ma et al., 2013). Heidelberg University (Ulrich Platt, personal communication, 2011) operates about 10 instruments, and the Anhui Institute of Optics and Fine Mechanics (AIOFM) runs more than 10 instruments within China (Wenqing Liu, personal communication, 2011), using a similar concept.

A major purpose of our network observations is to retrieve TropoNO2VCDs (and their vertical profiles) in the daytime to validate satellite observations at several key locations with different levels of air pollution, i.e., at Yokosuka, Cape Hedo, and Fukue (Japan), Gwangju (Korea), Hefei (China), and Zvenigorod and Tomsk (Russia). In addition, we aim to observe diurnal variations and vertical distributions of NO_2, beyond the capabilities of current satellite sensors on sun-synchronous orbits with fixed local time observations. We also aim to validate tropospheric chemical transport model simulations using the long-term record.

In this paper, we describe instrumental aspects of the network observations, features of temporal variations in the retrieved TropoNO2VCD data during 2007–2012 (for 3 to more than 5 yr of observations for each site), and comparisons with Ozone Monitoring Instrument (OMI) satellite observations and global model simulations. The instruments used at the individual sites were standardized so that the basic optical components used were the same. The obtained spectra were processed centrally to maintain homogeneous data quality over the sites. Temporal variations from diurnal,

ACPD
14, 2883–2934, 2014

weekly, seasonal, to multi-year scales were investigated, and compared with satellite observations wherever possible.

2 Experimental

2.1 Instrumentation

The MAX-DOAS instruments deployed at our network sites consisted of a light-receiving part and a miniature spectrometer connected by a bundle optical fiber cable (Fig. 1). The spectrometers used were USB4000 (Ocean Optics, Dunedin, FL, USA) equipped with a linear array of CCD detectors with 3648 pixels (TCD1304AP; Toshiba, Tokyo, Japan), except for the #1 instrument at Fukue, which was used for only 2 months (see Table 1), where another miniature spectrometer (BTC111; B&W TEK Inc., Newark, DE, USA) was used. The light-receiving part incorporated a flat rectangular mirror, with a 45° incidence angle, located in a weather-shielding quartz tube cap, and a telescope with a single plano-convex quartz lens of diameter 25 mm and a focal length of 40 mm. The telescope was coupled with an optical bundle fiber cable (length 1 m or 5 m) via an SMA (subminiature version A) connector, which consisted of seven cores (each with a diameter of 100 µm and a numerical aperture of 0.22). The cores formed a circle at the telescope side end and were aligned vertically at the exit, to fit to the slit shape of the spectrometer. The telescope restricted the field of view angle to less than 1°. The field of view angle was tested by introducing light into the fiber retrospectively from the exit side, and the divergence of the light after exiting the telescope was evaluated.

The rectangular mirror was rotated every 5 min to introduce scattered sunlight from the sky, with sequential elevation angles (ELs) of 3, 5, 10, 20, 30, and 90°, to the spectrometer through the telescope and the fiber bundle. One cycle of observations at six ELs (with integration for 5 min for each EL) took 30 min. The cycle was repeated on a 24 h basis. The spectrometer integration time was fixed at a value between 100 and 400 ms during the day and night. The integration time changed seasonally so that the

ACPD
14, 2883–2934, 2014

maximum signal level reached the middle range (between 20 000 and 40 000) of the full dynamic range of the 16-bit A/D converter (2^{16} = 65 536). A spectrum with a customized integration time was averaged over 250–600 integration times so that a single average spectrum was recorded every minute.

The spectrometer was located either in a light-receiving unit located outdoors (for the #2 instrument at Fukue, #1 and #2 instruments at Gwangju and Hefei, and for the single instruments used at Zvenigorod and Tomsk; see Table 1), in a customized thermoelectrically controlled refrigerator (for the single instruments used at Yokosuka and Hedo for the whole period) located indoors, or in a separate case (for the #3 instruments used at Fukue and Gwangju) located indoors. In all cases, the temperature of the spectrometer was stabilized to within ±0.2 °C using a temperature controller (KT4; Panasonic, Kadoma, Japan); the set temperature was 25–30 °C in winter and 35–45 °C in summer for the first case, 20 or 25 °C for the whole year for the second case, and 40 °C for all seasons for the last case. The precise temperature stabilization on a 24 h basis was important for the purpose of subtracting the dark spectrum measured during the night from the daytime spectra. A large part of the pixel-to-pixel pattern variability in the dark spectrum was constant over time, as long as the temperature was constant. For example, in the case of 38 °C, the pixel-to-pixel variability was as much as 96 digits as a standard deviation (1σ), for a spectrum obtained with an integration time of 100 ms averaged 600 times. However, after subtraction of the averaged dark "pattern" spectrum, recorded during the night-time, the random noise (pixel-to-pixel) was as small as 2–3.5. A signal-to-noise ratio of the order of 10^4 was therefore expected, which was typically required to analyze weak absorptions (< 0.1 %) quantitatively. Temperature stabilization was also important for keeping the wavelength shift constant over a long time period.

The USB4000 spectrometers used a standard grating (#5, a holographic grating for UV, with a groove density of 1200). The linear array CCD detector used the manufacturer's upgraded quartz window with UV transmittance and a cylindrical lens to enhance the efficiency. The slit width was generally 25 µm, except for the instrument installed at

ACPD
14, 2883–2934, 2014

Cape Hedo, which had a slit width of 10 µm. The spectrometers were customized so that a wavelength range from 230 to 560 nm was covered and a wavelength resolution below 0.7 nm in full-width at half-maximum (FWHM) was attained at the 407.783-nm mercury line. The resulting wavelength resolution in the 460–490 nm range, used for the analysis of NO_2 and O_4 in this study, was observed to be between 0.4 and 0.7 nm. The spectrometer was further customized to improve coupling to the fiber cable: a key lock, normally used to reproduce the angular position of the linearly aligned fiber cores at the exit of the bundle cable (within the SMA connector) with respect to the slit vertically oriented at the spectrometer, was removed and the connection was manually optimized in the rotational direction. The distance from the fiber end to the spectrometer slit was simultaneously optimized by inserting thin nylon spacers into the bottom space of the ferrule of the SMA connector at the exit end of the fiber. Thus, in addition to wavelength resolution, the spectral symmetry (determining the slit function shape) was optimized at a mercury line (407.783 nm) for each instrument before installation. The original distance between the fiber end and the slit determined by the manufacturer was often too short to optimize the spectral symmetry, although the signal intensity was higher there than that at our optimized position.

Single-notch filters at 405, 442, 488, and 355 nm (NF03-405E-25, NF01-442U-25, NF03-488E-25; Semrock Inc., Rochester, NY, USA) with a blocking optical depth (OD) > 6 and FWHM in the range of 9–14 nm, and a 355-nm notch-filter (Edmund Optics, Barrington, NJ, USA) with a blocking OD > 4 and FWHM of 18 nm, were used for stray-light characterization of the instrument. For typical daylight conditions, the stray light levels were estimated to be only 0.6–1.0 % of the daylight signal levels at each wavelength.

The ELs need to be absolutely accurate. The base plate of the light-receiving unit, to which the central axis of the telescope was parallel, was first set to be horizontal, using a horizontal level embedded in the base plate (Fig. 2). Subsequently, the angular position of the reflecting mirror at EL = 0° was carefully adjusted. A stepping motor (with an angle step of 0.038°), used for controlling the mirror angle, was equipped with an opti-

ACPD
14, 2883–2934, 2014

cal angular position sensor, with which the zero position was first roughly determined. Then, an additional offset angle (at a resolution of 0.1°) with respect to the sensor position was precisely adjusted until the reflecting mirror became fully horizontal. The offset angle thus determined was registered in the initial file of the software for the mirror rotation and was activated all the time. In this procedure, we used a second horizontal level (Fig. 2) embedded in a plate holding the reflecting mirror at a perpendicular angle. The level was easily seen from the top of the instrument through the quartz cap, facilitating setup in the field. All the ELs used for the observations were determined in this way relative to the zero position initially set at installation. The long-term drift (over more than 1 yr) of the zero position was typically less than 0.2°.

A laptop computer was used to control the mirror rotation and to collect all the spectra and house-keeping information (e.g., temperature control). A small fan was present beneath the quartz tube cap to avoid sedimentation of large aerosol particles on the surface of the cap, to remove small water droplets/snowflakes, and to reduce the possibility of small animals (e.g., spiders) interfering with the observations.

2.2 Observation sites

The instruments were deployed at seven locations (Figs. 3 and 4): at Cape Hedo (26.87° N, 128.25° E, 68 m a.s.l.), Okinawa Island, southwest of Japan, in March 2007, at Yokosuka, Japan (35.32° N, 139.65° E, 10 m) in April 2007, at Gwangju (35.23° N, 126.84° E, 43 m), Korea in February 2008, at Hefei, Anhui Province, China (31.91° N, 117.16° E, 51 m) in March 2008, at Zvenigorod, Russia (55.70° N, 36.78° E, 208 m) in October 2008, at Tomsk, Russia (56.48° N, 85.05° E) in January 2009, and at Fukue Island, Nagasaki Prefecture, west of Japan (32.75° N, 128.68° E, 80 m) in February 2009. The azimuth angle of the line of sight for each observation site is also listed in Table 1. The Yokosuka site (about 30 km south of Tokyo) is located within an industrialized area that extends in the north–south direction along Tokyo Bay in the Kanto Plain. The optical receiving part was located on top of a two-story building in our JAMSTEC headquarters campus. Cape Hedo is a remote site, located in the northern-most part of

ACPD
14, 2883–2934, 2014

subtropical Okinawa Island (Takami et al., 2007; Kanaya et al., 2001), and is distant from major cites (40 km from Nago, population 60 000 and 100 km from Naha, population 320 000 population). The instrument was located on top of a single-story building to house a lidar system of the Cape Hedo Aerosol and Atmosphere Monitoring Station, owned by the National Institute for Environmental Studies, Japan. For these two sites, five-fold optical axes were prepared for simultaneous observations at different ELs during intensive campaign periods. Under normal long-term operation, however, only a single telescope was used and the ELs were sequentially scanned. Observations at Gwangju were performed on the rooftop of the Samsung Environmental Research Building (32 m above sea level) at the Gwangju Institute of Science and Technology, 8 km north-northwest of the Gwangju city center (population 1.4 million). The observations at Hefei were performed on the rooftop of a five-story building of the AIOFM, about 10 km northwest of the Hefei city center (population 4.4 million). The Gwangju and Hefei sites are located at the edges of major city areas and are regarded as suburban sites. The observations at Zvenigorod were made on the rooftop of an observatory building of the Zvenigorod Research Station, affiliated to the Institute of Atmospheric Physics, Russian Academy of Sciences (Yurganov et al., 2010). The observatory is registered as a Network Detection of Atmospheric Composition Change site with respect to stratospheric NO_2 observations. The site is located in a rural area $\sim$ 50 km west of Moscow, whose population is $\sim$ 10.5 million. The observations at Tomsk were made on top of a research building (with five stories) of the Institute of Atmospheric Optics, Siberian Branch of the Russian Academy of Sciences. The site is $\sim$ 5 km east of the Tomsk city center, whose population is 520 000. For the two instruments located in Russia, the heat insulation was strengthened to tolerate low ambient temperatures during winter (between –20 and –40 °C). The data from Tomsk are still being evaluated, and will not be used in the following discussions. The differences of the local time (LT) from UTC are +9 h for Cape Hedo, Yokosuka, Fukue and Gwangju, +8 h for Hefei, and +4 h for Zvenigorod.

ACPD
14, 2883–2934, 2014

2.3 Retrieval algorithms

The recorded spectra were processed centrally so that the network observations produced data of homogeneous quality. The retrieval algorithm was similar to that used for JM1 (Irie et al., 2011), but (1) QDOAS software ver. 2.00 (http://uv-vis.aeronomie.be/software/QDOAS/, Fayt and Roozendael, 2012) was used for DOAS analysis, and (2) a newly coded Fortran program was used for subsequent conversion of the differential slant column densities (ΔSCDs) to vertical quantities. The basic flow of the analysis was similar to that used previously (Irie et al., 2008a, b, 2009a). Briefly, the measured spectra of scattered sunlight in the range of 460–490 nm at low ELs were analyzed, using the DOAS technique (Platt, 1994), to retrieve the ΔSCDs of oxygen collision complexes (O_2–O_2 or O_4) and NO_2 with respect to the reference spectrum obtained at the highest EL (90° or 70°). A reference spectrum was derived by interpolating two spectra measured within 30 min before and after the off-axis measurement. The absorption by gaseous species, i.e., O_4, NO_2, O_3, and H_2O, and the Ring effect were taken into account. The absorption cross-sections used were those reported by Herman et al. (http://spectrolab.aeronomie.be/o2.htm) for O_4, Vandaele et al. (1996) for NO_2 at 298 K, Bogumil et al. (2003) for O_3 at 223 K, and Rothman et al. (2003) for H_2O. The cross-sections of O_4 were increased by a factor of 1.25, following Clémer et al. (2010). A polynomial degree of three was used to fit the continuum. Typical residuals of spectral fitting were in the range of (5–20) × 10^{-4} for clear midday periods, but they increased in the early morning and late evening.

The O_4ΔSCD values were next converted to the AODs and vertical profiles of the aerosol extinction coefficients, using the optimal estimation method (OEM) developed by Rodgers (2000). The measurement vector consisted of five O_4ΔSCD values observed at low ELs. The state vector consisted of the AOD and three parameters (f_1, f_2, and f_3) determining the vertical profiles, with which the partial optical depths for the altitude ranges 0–1, 1–2, and 2–3 km were expressed as $f_1 \cdot$ AOD, $(1 - f_1) \cdot f_2 \cdot$ AOD, and $(1 - f_1) \cdot (1 - f_2) \cdot f_3 \cdot$ AOD, respectively (see Irie et al., 2008b). The a priori values and the

ACPD
14, 2883–2934, 2014

errors in the AOD, f_1, f_2, and f_3 were chosen to be 0.21±3.0, 0.60±0.05, 0.80±0.03, and 0.80±0.03, respectively. A lookup table of box air mass factors (A_{box}), which characterized the ratio of the partial slant to the vertical columns for a given layer, was created using a three-dimensional Monte Carlo radiative transfer model, MCARaTS (Iwabuchi, 2006). A_{box} calculations using MCARaTS have been validated through comparisons with other radiative transfer models (Wagner et al., 2007). An optimal aerosol (and A_{box}) profile scenario that accounted for the O_4ΔSCD values measured at all ELs was determined.

Using the A_{box} profiles and an iterative inversion method similar to that used for aerosol retrieval, a set of NO_2ΔSCD values for low ELs (as the measurement vector) was then converted to a tropospheric VCD and a vertical profile of NO_2 using an OEM. The state vector included TropoNO2VCD, and the partial fraction parameters v_1, v_2, and v_3, with which the partial NO_2 VCDs in the altitude ranges 0–1, 1–2, and 2–3 km were expressed as TropoNO2VCD$\cdot v_1$, TropoNO2VCD$\cdot(1-v_1)\cdot v_2$, and TropoNO2VCD$\cdot(1-v_1)\cdot(1-v_2)\cdot v_3$, respectively. The a priori values for TropoNO2VCD, v_1, v_2, and v_3 were selected to be 20 % of the largest ΔSCD values for NO_2, 0.60 ± 0.05, 0.80 ± 0.03, and 0.80 ± 0.03, respectively. The NO_2ΔSCD determinations using an instrument of the same design were validated during the CINDI 2009 (Cabauw Intercomparison Campaign of Nitrogen Dioxide measuring Instruments) campaign performed at Cabauw, the Netherlands, during June–July 2009 (Roscoe et al., 2010; Piters et al., 2012). The compatibility of the TropoNO2VCD data with those derived using the JM1 algorithm (Irie et al., 2011) was also confirmed.

Takashima et al. (2009) established an original cloud-screening method for studying aerosols at Cape Hedo using a combination of the MAX-DOAS color index (defined as the ratio of the intensities at 500 and 380 nm) and the relative humidity, derived from H_2O retrieved from the MAX-DOAS analysis. However, for the retrieval of NO_2, which is the main target of this study, critical cloud screening using the color index was not applied, because the NO_2 state would be retrieved properly as long as the optical path length was determined correctly. It should also be noted that even without

ACPD
14, 2883–2934, 2014

such screening using the color index, a large fraction of cloudy cases was eliminated in advance, as the observed $O_4\Delta$SCD values at five ELs were irregularly distributed and were not well fitted. See the Supplement for details of cloud screening using the color index applied for the evaluation of the retrieved aerosol quantities.

Error estimation methodologies have been reported for random and systematic uncertainties in aerosol retrievals (Irie et al., 2008a; Takashima et al., 2009). The overall uncertainty in the AOD was estimated from our past comparisons with existing methods (sky radiometer and Mie lidar) to be 30 %. The method used to calculate random and systematic uncertainties in TropoNO2VCD has been described elsewhere (Irie et al., 2009a, 2011). The random uncertainty was estimated to be 10 %, based on the residuals in the ΔSCD fitting. The systematic error was estimated to be 14 %, to which the uncertainties in the AOD and in the A_{box} contributed by similar degree. The combined total uncertainty was typically 17 %. Takashima et al. (2011, 2012) reported that similar instruments had detection limits for NO_2 mixing ratios of < 0.2 ppb at an altitude of 0–1 km, corresponding to a minimum detectable TropoNO2VCD of $< 5 \times 10^{14}$ molecules cm^{-2}.

Figure 5 demonstrates the performance of our retrievals for selected morning hours [08:00–09:00 (8 h) or 09:00–10:00 (9 h), LT], and afternoon hours [15:00–16:00 (15 h) or 16:00–17:00 (16 h) LT] in June at three locations (Zvenigorod, Hefei, and Yokosuka). The $O_4\Delta$SCD values (Fig. 5a–c) showed negative dependences on the ELs, and they were well fitted using the OEM. The low $O_4\Delta$SCD values at Hefei at all ELs (Fig. 5b) were explained by the presence of dense aerosols. The $O_4\Delta$SCD values in the afternoon were higher at Hefei (Fig. 5b) and Yokosuka (Fig. 5c), and lower at Zvenigorod (Fig. 5a), than those in the morning; this was mainly explained by differences among the relative azimuth angles of observation. The retrieved AOD values were similar for the morning and afternoon at all the sites. The $NO_2\Delta$SCD values were higher in the morning than in the afternoon in all cases (Fig. 5d–f), because NO_2 was more abundant in the morning. At Zvenigorod and Hefei, the $NO_2\Delta$SCD values showed a stronger dependence on the EL in the morning than in the afternoon, resulting in steeper ver-

ACPD
14, 2883–2934, 2014

tical profiles (and higher v_1 values) in the morning (Fig. 5g and h). At Yokosuka, the dependence of the $NO_2\Delta SCD$ values on EL did not greatly change from the morning to the afternoon, and therefore the v_1 values and the vertical profiles of NO_2 were almost unchanged diurnally. This could be explained by continuous NO_x emissions from nearby sources at Yokosuka, sustaining a relatively steep vertical gradient at all times. In contrast, the less steep vertical gradients in NO_2 up to 2 km at Zvenigorod and Hefei in the afternoon could be explained by the fact that nearby sources were less important, and that the continental boundary layer height became thicker in the afternoon during summer. The degrees of freedom of the signal typically exceeded two during the daytime periods between the morning and afternoon hours studied here.

The final products of our retrieval were TropoNO2VCDs, AODs, vertical profiles of NO_2 and extinction coefficients, with a resolution of 1 km (up to 3 km) at a time resolution of 30 min during daytime. Careful quality control of the data was applied to remove cases with wrong mirror operations, power blackouts, shifts in the dark spectra as a result of changes in integration time and temperature settings, large residuals in the spectral fittings, malfunction in the temperature control, and saturated signal levels.

3 Results and discussion

We focus on NO_2 in this paper, so evaluation of our AOD results is included in the Supplement. The NO_2 data obtained at Yokosuka and Hedo have been partly used for validation of TropoNO2VCD derived from OMI and other satellite sensors (Irie et al., 2009a, 2012), comparisons with ship-based observations (Takashima et al., 2012), and for analysis of transport from the Asian continent (Takashima et al., 2011). In this paper, independently of previous papers, we focus on features of temporal variations at multiple time scales (e.g., diurnal, weekly, and seasonal variations) of TropoNO2VCD. Comparisons with satellite-based TropoNO2VCD are also made wherever possible. Finally, we include comparisons with the simulation results from a global chemical transport model at Cape Hedo and Fukue.

ACPD
14, 2883–2934, 2014

3.1 Variations on seasonal or longer scales: comparisons with OMI

Figure 6 shows the full records of the TropoNO2VCDs for all the sites, including data during the whole daytime period, until December 2012. Table 1 summarizes the number of successful NO_2 retrievals for each site; in total, 80 927 data are included in the analysis in this paper. They are subsets of 180 654 data for which ΔSCDs of NO_2 and O_4 for all ELs were successfully determined and 90 644 data for which aerosol retrievals were successful, after careful data screening with respect to the instrumental conditions. The VCD levels were highest (at around 10^{16}–10^{17} molecules cm^{-2}) at Yokosuka, an urban site, and lowest (at around 3×10^{14} to 5×10^{15} molecules cm^{-2}) at Cape Hedo, a remote site; the VCD levels from other sites (Hefei, Gwangju, Zvenigorod, and Fukue, in descending order) were between these. Altogether, our TropoNO2VCD data ranged over more than two orders of magnitudes. The wide dynamic range and its full coverage were advantageous for the validation of satellite data, as shown later.

Figure 7 shows time series of monthly averaged MAX-DOAS observations (during 13:00–14:00 LT, except for 15:00–16:00 LT at Zvenigorod, matching satellite overpass timings) and satellite observations of TropoNO2VCD from the OMI sensor. For the OMI data, we used two different products, i.e., one derived from the algorithm developed by the National Aeronautics and Space Administration (NASA) and the other from the algorithm (Dutch OMI NO_2 (DOMINO)) developed by Koninklijk Nederlands Meteorologisch Instituut. The NASA data set was the ver. 2.1 release of the gridded OMNO2d daily level 3 products (OMNO2d.003), with cloud screening at 30 %, at a resolution of 0.25° × 0.25°, available from the NASA Giovanni website (http://gdata1.sci.gsfc.nasa.gov/daac-bin/G3/gui.cgi?instance_id=omi; Bucsela et al., 2013). The latter data set was the monthly DOMINO ver. 2.0 collection 3, at a resolution of 0.125°×0.125°, available from the Tropospheric Emission Monitoring Internet Service (TEMIS) website (http://www.temis.nl/airpollution/no2col/no2regioomimonth_col3.php; Boersma et al., 2011). The data at the nearest grid were used for both products. For the DOMINO algorithm, the results at eight adjacent grids were included (gray lines in

ACPD
14, 2883–2934, 2014

Fig. 7) in addition to the nearest grid, to represent the spatial inhomogeneity of NO_2 over the range 0.375° × 0.375°.

At Cape Hedo and Fukue, where the local sources were negligible and thus the observations were ideally representative over the grids described above (or over the footprint size of the satellite observations, i.e., 24 km × 13 km or larger), the concentration levels and variation patterns were in relatively good agreement (Fig. 7a and b). At the two sites, the previous data product from NASA (ver. 1) always yielded significantly higher levels (Fig. 7a and b). After revision of the data set, disagreements with the MAX-DOAS observations disappeared and the agreement improved. For relatively low ranges of TropoNO2VCD ($\lesssim 3 \times 10^{15}$ molecules cm^{-2}), precise subtraction of the stratospheric component of NO_2 is important for satellite observations; this might have been the source of differences, although full identification of the cause is beyond the scope of this paper.

The monthly variation pattern at Zvenigorod (Fig. 7f), in the middle range, i.e., $\sim 10 \times 10^{15}$ molecules cm^{-2}, is very well reproduced by the satellite observations. The satellite data capture the decreasing and increasing trends found using the MAX-DOAS observations from April to October in 2011 and 2012, respectively.

In contrast, in polluted areas with TropoNO2VCD values normally exceeding 10×10^{15} molecules cm^{-2}, for example, at Yokosuka and Gwangju (Fig. 7c and d), the MAX-DOAS observations tended to be higher than both satellite-derived values. The spatial variability of the NO_2 values over the nine grids for the DOMINO data set was relatively small and did not extend to the average levels of the MAX-DOAS observations in winter at Yokosuka. This may indicate that spatial inhomogeneity alone cannot explain the difference between the MAX-DOAS and satellite observations, although the inhomogeneity at scales smaller than 0.125° could be responsible for the differences. It should be noted that the MAX-DOAS observations are representative over a distance of about 2–10 km on the line of sight.

Figure 8a and b show summary scatterplots of the monthly averaged TropoNO2VCD values from observations by MAX-DOAS and those by OMI with two algorithms,

ACPD
14, 2883–2934, 2014

DOMINO ver. 2.0 and NASA ver. 2.1. The correlations were very tight for both cases, with R^2 values exceeding 0.84, suggesting that the two satellite-derived products captured monthly variations quite well. However, the slopes were ∼ 0.5 for both cases, suggesting that the satellite observations tended to give lower values than the MAX-DOAS observations did, and were strongly influenced by the data in the high range. The deviation from unity cannot be explained by the combined uncertainties in the satellite observations (∼ 25 %, Boersma et al., 2011) and MAX-DOAS.

When we limited the data to months where (1) more than 50 % of the days of satellite observations were overlapped with MAX-DOAS observations and vice versa, and (2) coincident observations were made on 5 or more days, the R^2 value became even larger (R^2 = 0.88), but the slope remained at around 0.5. When the observation sites were grouped into two types, i.e., urban/suburban (Yokosuka, Gwangju, and Hefei) and rural/remote (Zvenigorod, Fukue, and Cape Hedo), the slopes were almost unchanged (0.54) for the urban/suburban case, whereas those for the rural/remote type increased to 0.78 and 0.63 with R^2 values of 0.74 and 0.65, with respect to DOMINO and NASA products, respectively (Fig. 8c and d). This suggested the possibility that the observations at the three sites categorized as urban/suburban type did not represent the grids, and the spatial inhomogeneity could partly explain the larger departure of the slope value from unity.

This magnitude relationship was the opposite to those found in previous validation studies, which suggested the DOMINO products (ver. 1.02) had a high bias, i.e., 0–40 % (Hains et al., 2010; Huijnen et al., 2010; Lamsal et al., 2010; Zhou et al., 2009), as summarized by Boersma et al. (2011). The revisions from DOMINO ver. 1.02 to the current version (ver. 2.0) were too small at the three urban/suburban sites (i.e., Yokosuka, Gwangju, and Hefei) to explain the different results. However, recent studies suggested low biases, 26–38 % and ∼ 50 %, in Beijing and in Delhi and its surroundings, respectively (Ma et al., 2013; Shaiganfar et al., 2011), in agreement with the magnitude relationship we found for the three urban/suburban sites.

ACPD
14, 2883–2934, 2014

Figure 9 shows the scatterplots between MAX-DOAS and OMI satellite observations at satellite pixel levels ($n = 813$, for six sites altogether) using more strict coincidence criteria (horizontal displacement < 0.15°, time difference < 15 min) and cloud screening (cloud fraction < 10 %). This also resulted in a similar underestimation of TropoNO2VCD for the satellite data; the slopes were 0.53 and 0.46, against DOMINO (ver. 2.0) and NASA (ver. 2.1), respectively. The slopes for the three cleaner sites were similar (0.55 and 0.42, respectively). This analysis indicated that a slope value lower than unity cannot be attributed to the poor overlap of the measurement days in each month or to the spatial inhomogeneity down to the scales of the footprint size of the satellite observations.

Another possibility would be that systematic underestimation by satellite observations arises from assumptions in the vertical profiles and aerosol treatment. Figure 10a shows that low OMI(NASA)/MAX-DOAS ratios (using a gridded data set for OMI) are associated with high AODs (as observed by MAX-DOAS); although the median ratio is near unity at low AODs (~ 0.1), it becomes lower (~ 0.7) with AODs as high as 1. In this study, only data with more than 1×10^{15} molecules cm^{-2} for both MAX-DOAS and satellite observations are used. This suggests the possibility that the satellite observations underestimate TropoNO2VCD when aerosols are densely present. This is less likely to be explained by overestimation by MAX-DOAS at high AODs, where the effect is already taken into account more adequately. All of the data ($n = 1834$ from the six sites) were subdivided into two groups of equal size, based on AOD values (i.e., two groups with high and low AOD values) and a Welch's t test was applied. The results suggested that the OMI(NASA)/MAX-DOAS ratio was significantly lower for high AODs at the 95 % confidence level. Similar tests for individual sites led to the same conclusion for Fukue, Zvenigorod, and Gwangju. Figure 10b shows that the NASA(OMI)/MAX-DOAS ratio for TropoNO2VCD had a weak decreasing trend with the retrieved parameter v_1, the fraction of NO_2 present in the lowest 1 km. The median values decreased from around unity to 0.67 as v_1 increased from ~ 0.6 to 0.9. Welch's t tests applied to two groups of data sorted by v_1 values suggested that the ratio was significantly lower for the group

ACPD
14, 2883–2934, 2014

with higher v_1 values when using data from all six sites and when using data from Yokosuka and Hefei individually, at the 95 % confidence level. This suggests that the underestimation occurs when NO_2 is mostly present near the surface. These analyses, in combination, imply that the lower values from the satellite could be partly caused by the assumptions made regarding the vertical profiles and aerosol treatment in the satellite data analysis, especially at clean sites, where the spatial inhomogeneity cannot be responsible for the difference. For both satellite data products, air mass factors were computed as average of clear and cloudy conditions weighted by the cloud radiation fraction, and therein the aerosols are implicitly taken into account similarly to clouds (Boersma et al., 2011; Bucsela et al., 2013). Such corrections seemed almost successful in that AOD did not govern the variability of the ratio (Fig. 10a); however, a weak dependence on AOD was still discernible. Recently, Shaiganfar et al. (2011) and Ma et al. (2013) suggested that the shielding effect of NO_2 by aerosols could be significant for OMI observations, resulting in similarly low values. Lin et al. (2013) suggested that concentration of aerosols at the top of the boundary layer increased retrieved NO_2 by 8 %.

From the above analyses of correlations and dependences on AOD and v_1, we conclude that the values of the OMI satellite data for TropoNO2VCD were lower than those from the network MAX-DOAS observations, and were possibly affected by the presence of aerosols, the assumptions made regarding the vertical profile of NO_2, and how representative the site is (for the urban/suburban cases). Future satellite observations with smaller footprint sizes will improve the analysis.

Figure 11 shows the averaged seasonal variations in the MAX-DOAS and satellite-based observations. MAX-DOAS data recorded during 13:00–14:00 LT (15:00–16:00 LT for Zvenigorod), matching satellite overpass timings, were used. Here, the right-axis scales for the OMI-derived quantities were adjusted by factors of 1.23, 1.54, 1.76, 1.77, 1.71, and 1.07 for Cape Hedo, Fukue, Yokosuka, Gwangju, Hefei, and Zvenigorod, respectively. At almost all sites except Zvenigorod, TropoNO2VCD had a clear summer minimum and winter maximum. This feature can be interpreted using

ACPD
14, 2883–2934, 2014

a combination of (1) seasonal changes in NO_x emissions, (2) efficient partitioning to NO via faster photolysis rates of NO_2 in summer, and (3) efficient oxidation of NO_2 by OH in summer. Van der A et al. (2008) suggested, based on their analysis of GOME and SCIAMACHY (SCanning Imaging Absorption spectroMeter for Atmospheric CartograpHY) satellite data that the wintertime maximum indicates the dominance of NO_x sources from anthropogenic sectors (fossil fuel and biofuel combustion). Each of our observation sites had unique features in their seasonal patterns (Fig. 11), and the satellite data captured such detailed features quite well. For example, seasonal variations at Fukue Island and Hefei were relatively symmetric with respect to June/July. At Yokosuka and Gwangju, decreases in spring were slow, but increases in fall were relatively rapid. The wintertime peak occurred in December at Gwangju, whereas it appeared in January at Hefei. At Zvenigorod, low levels lasted for a short period during June–August, and the values in April and May, and in October, were larger. All these detailed features were quite well reproduced by the satellite observations.

The observed features in the year-to-year variations were also well reproduced by the satellite observations (Fig. 7). For example, relatively high values in January 2011 at Cape Hedo, and those in December 2009 and January 2010 at Fukue were well captured.

3.2 Diurnal and weekly variations

Figure 12 shows the diurnal variations averaged for each month. Generally, daytime decreases were recorded, as a result of (1) stronger emissions in the early morning, (2) effective partitioning to NO in the daytime by NO_2 photolysis, and (3) stronger oxidation of NO_2 by OH, similar to the causes for the summer minima. At Cape Hedo, such a pattern of daytime decreases was clearly seen for all months (Fig. 12a). In contrast, at Yokosuka, Gwangju, and Hefei (Fig. 12c–e) in winter, daytime increases in TropoNO2VCD were observed. The periods with daytime increases were November–February at Yokosuka, November–December at Gwangju, and December–January at Hefei, slightly different from site to site. This feature was interpreted as (1) accumu-

ACPD
14, 2883–2934, 2014

lation of pollutants overriding the loss rates and/or (2) importing of more polluted air masses in the afternoon period. Particularly at Yokosuka, located about 30 km south of the Tokyo metropolitan area, the wintertime northerly wind tended to carry more polluted air masses from northern areas near Tokyo to the south, resulting in higher NO_2 concentrations in the afternoon. Similar daytime increases in TropoNO2VCD during winter were reported in Greenbelt, Maryland, USA (Wenig et al., 2008) and in/near Beijing, China (Ma et al., 2013; Hendrik et al., 2013). Figure 13a shows that the diurnal variation patterns for the partial column of NO_2 in the 0–1 km altitude range in four selected months, January, April, July, October at Yokosuka, are quite similar to those for NO_2 measured at a nearby air-quality-monitoring site (Nagahama site, about 4 km to the northwest). The NO_2 monitoring was performed using a chemiluminescence instrument equipped with a molybdenum converter, and thus was potentially influenced by other NO_z species; in the urban locations near Tokyo, however, the influence was small (e.g., Kondo et al., 2008). In this study, we only compared the diurnal patterns. In the afternoons in January, the patterns were significantly different. The air mass on the line of sight of MAX-DOAS over Tokyo Bay could have been more influenced by the transport of polluted air masses from the Tokyo region or by ship emissions in the afternoon in winter.

Figure 14 shows the diurnal variations averaged separately for each day of the week. Apparent holidays for each country were re-categorized as Sundays. Although almost no weekend reductions were observed at remote locations (Cape Hedo and Fukue, Fig. 14a and b), the TropoNO2VCD values were clearly lower on Sundays at Yokosuka and Gwangju, because of the lower emissions from nearby sources, primarily as a result of less traffic (e.g., diesel trucks). At a similar suburban site, i.e., Hefei, however, this weekly cycle was not observed (Fig. 14e). This different behavior suggests that the NO_x emission rate from the major sector there does not follow a weekly cycle. It has been estimated from an Asian emission inventory for INTEX-B for 2006 that 24, 58 and 61 % of NO_x emission are from the transportation sector for China, Korea, and Japan, respectively (Zhang et al., 2009). The lower contribution from the transport sector for

ACPD
14, 2883–2934, 2014

China probably causes this difference. The negligible weekly variation in China was consistent with the results of an earlier study using GOME data (Beirle et al., 2003). Similar results without weekend anomalies were found by Ma et al. (2013) for MAX-DOAS observations in Beijing.

Figure 13b shows that the average diurnal profiles of the partial vertical columns of NO_2 in the 0–1 km altitude range for weekdays, Saturdays, and Sundays at Yokosuka are in nearly perfect agreement with those for NO_2 monitoring at the Nagahama site. These analyses of diurnal and weekly behaviors of NO_2 help to refine the emission inventory of NO_x. For the Kanto area, including Yokosuka and Tokyo, NO_x emissions on Sundays were estimated to be lower by 45 % (Kannari et al., 2007) for the year 2000, which is roughly in agreement with our observations (37 % reduction on Sundays for 07:00–16:00 LT). A more detailed comparison between observed and modeled NO_2 at Yokosuka is planned, to refine the emission inventories and to test the unique wintertime diurnal variation there.

Figure 15 compares the MAX-DOAS-derived reduction ratios for TropoNO2VCD at weekends (for Saturdays and Sundays separately) with respect to weekdays, during 13:00–14:00 LT (15:00–16:00 LT for Zvenigorod), with those from OMI satellite observations (using the NASA algorithm). The reduction ratios for Yokosuka, Gwangju, and Zvenigorod for Sundays were 0.57, 0.89, and 0.71 for OMI, similar to 0.59, 0.76, and 0.85 for MAX-DOAS. On Saturdays, the reduction ratios were commonly larger, and were almost unity at Zvenigorod. The ratios for MAX-DOAS at Hefei were somewhat larger, but this could be a result of the small number of data available for this specific hour.

3.3 Comparison with model simulations

The climatology based on the TropoNO2VCD values observed with MAX-DOAS at Cape Hedo and Fukue, relatively remote locations, was compared with the simulation results derived from a global chemical transport model, MIROC-ESM-CHEM (Watanabe et al., 2012), based on CHASER (Sudo et al., 2002), to evaluate the model simula-

ACPD
14, 2883–2934, 2014

tions. The model included stratospheric/tropospheric chemistry and aerosol schemes, and had a spatial resolution of 2.8° × 2.8° and 32 vertical layers. The wind field was assimilated using National Centers for Environmental Prediction data. HadISST/ICE (http://badc.nerc.ac.uk/view/badc.nerc.ac.uk__ATOM__dataent_hadisst) data were used for the sea surface temperature. The simulations were made for 6 yr (2007–2012) and the average seasonal and diurnal variations were compared with the observations. The used emission inventory was derived from Cofala et al. (2007), but the baseline year was updated to 2005. The NO_x emissions and concentrations in east Asia could therefore be underestimated for the study period, because the emission rates have increased since 2005.

In Fig. 16, seasonal variations in TropoNO2VCD at different sites during 13:00–14:00 LT are compared. For Cape Hedo, the concentrations in all seasons except winter were quite well reproduced by the model simulations. To our knowledge, this is the first use of the climatology of TropoNO2VCD values in such a low range, as observed at remote islands, to evaluate global chemical transport model simulations. The seasonal variations, with summertime minima and wintertime maxima, were also well reproduced, although the model tended to underestimate wintertime values. Similar features were observed in the comparison with Fukue Island (Fig. 16b), where the wintertime underestimation was more significant than that for Cape Hedo. Because Fukue Island is located nearer to NO_x source regions in the Asian continent (including the Korean Peninsula), possible underestimation of NO_x emissions on the continent could explain the differences during the winter, when air masses generally originate from the Asian continent. In contrast, during summer, clean air masses reached the two sites from the open Pacific Ocean. Our results therefore suggested that the model simulation is valid in summer under such conditions, where the TropoNO2VCD values were as low as 0.6–1.5 × 10^{15} molecules cm^{-2}.

Figure 17 compares the observed and modeled diurnal variations of TropoNO2VCD during four seasons. At Cape Hedo, the concentrations and detailed diurnal patterns, including daytime decreases and their rates in June–August (JJA) and September–

ACPD
14, 2883–2934, 2014

November (SON), were almost perfectly reproduced by the model simulations. For Fukue, the rate of decrease at midday in JJA was also well captured by the model. This analysis again indicated that the NO_2 chemistry during the daytime was well simulated in the model, especially in summer.

3.4 Data availability

Numerical data files for the MADRAS network observations are available at http://ebcrpa.jamstec.go.jp/maxdoashp. The files include TropoNO2VCD, AOD, vertical profiles of NO_2, and extinction coefficients, with a 1 km resolution (up to 3 km) and a time resolution of 30 min. The color index information is also included (see the Supplement for details).

4 Summary

Long-term network observations of TropoNO2VCD were conducted at seven sites, in Japan, Korea, China, and Russia, covering remote to urban areas, from 2007, using standardized MAX-DOAS instruments. A single algorithm was applied to the raw spectra obtained at the sites to derive the ΔSCDs of NO_2 and O_4, and to estimate TropoNO2VCD optimally, using the aerosol information derived from the O_4 observations. A large number (> 80 000) of the TropoNO2VCD values were used to test satellite observations of TropoNO2VCD from OMI and model simulations, and to investigate the climatology of NO_2. The results were similar for two satellite data products with different retrieval algorithms (DOMINO ver. 2.0 and NASA ver. 2.1); the satellite observations had low biases, i.e., ∼ 50 %, whereas they were tightly correlated with the MAX-DOAS observations and showed closely matching seasonalities. Our analysis showed that the low biases could be attributed to the inhomogeneity of NO_2 on the spatial scale of the data products from OMI observations, and incomplete accounting for NO_2 present near

ACPD
14, 2883–2934, 2014

the surface, possibly related to the shielding effect caused by the co-existing aerosols, for the satellite observations.

The average diurnal variations in TropoNO2VCD generally showed daytime decreases during the summer but increases during the winter at urban/suburban sites. Weekend reductions in NO_2 were clearly seen at Yokosuka and Gwangju, as a result of a reduction in the amount of traffic, but did not occur at Hefei, China, where the major emitting sector was probably different. The diurnal and weekly cyclic patterns at Yokosuka were in good agreement with those derived from ground-based-monitoring data recorded near the site. A global chemical transport model, MIROC-ESM-CHEM, was validated for the first time with respect to background-level NO_2 column densities at Cape Hedo and Fukue during the summer, under the influence of marine air masses from the Pacific Ocean.

Supplementary material related to this article is available online at http://www.atmos-chem-phys-discuss.net/14/2883/2014/acpd-14-2883-2014-supplement.pdf.

Acknowledgements. We thank Prede Co., Ltd. for technical assistance in developing instruments. Support from Y. Takeda and M. Kubo at the observatory is gratefully acknowledged. A. Takami and A. Shimizu (National Institute of Environmental Studies), T. Takamura (Chiba University), Y. Komazaki (Japan Agency for Marine and Earth Science and Technology) logistically supported our observations. We are grateful for free use of tropospheric NO_2 column data from the OMI sensor from www.temis.nl and from NASA. This work was supported by the Environmental Research and Technology Development Fund (S-7) of the Ministry of the Environment, Japan, by the Japan EOS Promotion Program (JEPP) of the Ministry of Education, Culture, Sports, Science, and Technology in Japan, by JSPS and RFBR (research project No. 12-05-92108_Jap_a and 11-05-01175-a) under the Japan-Russia Research Cooperative Program, and by the GEMS program of the Ministry of Environment, Korea and the Eco Innovation Program of KEITI (2012000160004).

ACPD
14, 2883–2934, 2014

References

Beirle, S., Platt, U., Wenig, M., and Wagner, T.: Weekly cycle of NO_2 by GOME measurements: a signature of anthropogenic sources, Atmos. Chem. Phys., 3, 2225–2232, doi:10.5194/acp-3-2225-2003, 2003.

Boersma, K. F., Eskes, H. J., Veefkind, J. P., Brinksma, E. J., van der A, R. J., Sneep, M., van den Oord, G. H. J., Levelt, P. F., Stammes, P., Gleason, J. F., and Bucsela, E. J.: Near-real time retrieval of tropospheric NO_2 from OMI, Atmos. Chem. Phys., 7, 2103–2118, doi:10.5194/acp-7-2103-2007, 2007.

Boersma, K. F., Eskes, H. J., Dirksen, R. J., van der A, R. J., Veefkind, J. P., Stammes, P., Huijnen, V., Kleipool, Q. L., Sneep, M., Claas, J., Leitão, J., Richter, A., Zhou, Y., and Brunner, D.: An improved tropospheric NO_2 column retrieval algorithm for the Ozone Monitoring Instrument, Atmos. Meas. Tech., 4, 1905–1928, doi:10.5194/amt-4-1905-2011, 2011.

Bogumil, K., Orphal, J., Homann, T., Voigt, S., Spietz, P., Fleischmann, O. C., Vogel, A., Hartmann, M., Bovensmann, H., Frerik, J., and Burrows, J. P.: Measurements of molecular absorption spectra with the SCIAMACHY Pre-Flight Model: Instrument characterization and reference spectra for atmospheric remote sensing in the 230–2380 nm region, J. Photochem. Photobiol. A, 157, 167–184, 2003.

Brinksma, E. J., Pinardi, G., Volten, H., Braak, R., Richter, A., Schönhardt, A., van Roozendael, M., Fayt, C., Hermans, C., Dirksen, R. J., Vlemmix, T., Berkhout, A. J. C., Swart, D. P. J., Oetjen, H., Wittrock, F., Wagner, T., Ibrahim, O. W., de Leeuw, G., Moerman, M., Curier, R. L., Celarier, E. A., Cede, A., Knap, W. H., Veefkind, J. P., Eskes, H. J., Allaart, M., Rothe, R., Piters, A. J. M., and Levelt, P. F.: The 2005 and 2006 DANDELIONS NO_2 and aerosol intercomparison campaigns, J. Geophys. Res., 113, D16S46, doi:10.1029/2007JD008808, 2008.

Bucsela, E. J., Perring, A. E., Cohen, R. C., Boesma, K. F., Celarier, E. A., Gleason, J. F., Wenig, M. O., Bertram, T. J., Wooklridge, P. J., Dirksen, R., and Veefkind, J. P.: Comparison of tropospheric NO_2 from in situ aircraft measurements with near-real-time and standard product data from OMI, J. Geophys. Res., 113, D16S31, doi:10.1029/2007JD008838, 2008.

Bucsela, E. J., Krotkov, N. A., Celarier, E. A., Lamsal, L. N., Swartz, W. H., Bhartia, P. K., Boersma, K. F., Veefkind, J. P., Gleason, J. F., and Pickering, K. E.: A new stratospheric and tropospheric NO_2 retrieval algorithm for nadir-viewing satellite instruments: applications to OMI, Atmos. Meas. Tech., 6, 2607–2626, doi:10.5194/amt-6-2607-2013, 2013.

ACPD
14, 2883–2934, 2014

Burrows, J, P., Weber, M., Buchwitz, M., Rozanov, V., Ladstätter-Weißenmayer, A., Richter, A., DeBeek, R., Hoogen, R., Bramstedt, K., Eichmann, K- U., Eisinger, M., and Perner, D.: Global Ozone Monitoring Experiment (GOME): mission concept and first scientific results, J. Atmos. Sci., 56, 171–175, 1999.

Celarier, E. A., Brinksma, E. J., Gleason, J. F., Veefkind, J. P., Cede, A., Herman, J. R., Ionov, D., Goutail, F., Pommereau, J.-P., Lambert, J.-C., van Roozendael, M., Pinardi, G., Wittrock, F., Schönhardt, A., Richter, A., Ibrahim, O. W., Wagner, T., Bojkov, B., Mount, G., Spinei, E., Chen, C. M., Pongetti, T. J., Sander, S. P., Bucsela, E. J., Wenig, M. O., Swart, D. P. J., Volten, H., Kroon, M., and Levelt, P. F.: Validation of Ozone Monitoring Instrument nitrogen dioxide columns, J. Geophys. Res., 113, D15S15, doi:10.1029/2007JD008908, 2008.

Chen, D., Zhou, B., Beirle, S., Chen, L. M., and Wagner, T.: Tropospheric NO_2 column densities deduced from zenith-sky DOAS measurements in Shanghai, China, and their application to satellite validation, Atmos. Chem. Phys., 9, 3641–3662, doi:10.5194/acp-9-3641-2009, 2009.

Clémer, K., Van Roozendael, M., Fayt, C., Hendrick, F., Hermans, C., Pinardi, G., Spurr, R., Wang, P., and De Mazière, M.: Multiple wavelength retrieval of tropospheric aerosol optical properties from MAXDOAS measurements in Beijing, Atmos. Meas. Tech., 3, 863–878, doi:10.5194/amt-3-863-2010, 2010.

Cofala, J., Amann, M., Klimont, Z., Kupiainen, K., and Högund-Isaksson, L: Scenarios of global anthropogenic emissions of air pollutants and methane until 2030, Atmos. Environ., 41, 8486–8499, 2007.

Duce, R. A., LaRoche, J., Altieri, K., Arrigo, K. R., Baker, A. R., Capone, D. G., Cornell, S., Dentener, F., Galloway, J., Ganeshram, R. S., Geider, R. J., Jickells, T., Kuypers, M. M., Langlois, R., Liss, P. S., Liu, S. M., Middelburg, J. J., Moore, C. M., Nickovic, S., Oschlies, A., Pedersen, T., Prospero, J., Schlitzer, R., Seitzinger, S., Sorensen, L. L., Uematsu, M., Ulloa, O., Voss, M., Ward, B., and Zamora, L.: Impacts of atmospheric anthropogenic nitrogen on the open ocean, Science, 320, 893–897, 2008.

Fayt, C. and Van Roozendael, M.: QDOAS Software User Manual Version 2.00, available at: http://uv-vis.aeronomie.be/software/QDOAS/ (last access: April 2012), 2012.

Galle, B., Johansson, M., Rivera, C., Zhang, Y., Kihlman, M., Kern, C., Lehmann, T., Platt, U., Arellano, S., and Hidalgo, S.: Network for Observation of Volcanic and Atmospheric Change (NOVAC) – a global network for volcanic gas monitoring: network layout and instrument description, J. Geophys. Res., 115, D05304, doi:10.1029/2009JD011823, 2010.

ACPD
14, 2883–2934, 2014

Hains, J. C., Boersma, K. F., Kroon, M., Dirksen, R. J., Cohen, R. C., Perring, A. E., Bucsela, E., Volten, H., Swart, D. P. J., Richter, A., Wittrock, F., Schoenhardt, A., Wagner, T., Ibrahim, O. W., van Roozendael, M., Pinardi, G., Gleason, J. F., Veefkind, J. P., and Levelt, P.: Testing and improving OMI DOMINO tropospheric NO_2 using observations from the DANDELIONS and INTEX-B validation campaigns, J. Geophys. Res., 115, D05301, doi:10.1029/2009JD012399, 2010.

Hendrick, F., Müller, J.-F., Clémer, K., De Mazière, M., Fayt, C., Hermans, C., Stavrakou, T., Vlemmix, T., Wang, P., and Van Roozendael, M.: Four years of ground-based MAX-DOAS observations of HONO and NO_2 in the Beijing area, Atmos. Chem. Phys. Discuss., 13, 10621–10660, doi:10.5194/acpd-13-10621-2013, 2013.

Heue, K.-P., Richter, A., Bruns, M., Burrows, J. P., v. Friedeburg, C., Platt, U., Pundt, I., Wang, P., and Wagner, T.: Validation of SCIAMACHY tropospheric NO_2-columns with AMAXDOAS measurements, Atmos. Chem. Phys., 5, 1039–1051, doi:10.5194/acp-5-1039-2005, 2005.

Holben, B. N., Tanre, D., Smirnov, A., Eck, T. F., Slutsker, I., Abuhassan, N., Newcomb, W. W., Schafer, J., Chatenet, B., Lavenue, F., Kaufman, Y. J., Vande Castle, J., Setzer, A., Markham, B., Clark, D., Frouin, R., Halthore, R., Karnieli, A., O'Neill, N. T., Pietras, C., Pinker, R. T., Voss, K., and Zibordi, G.: An emerging ground-based aerosol climatology: aerosol optical depth from AERONET, J. Geophys. Res., 106, 12067–12097, 2001.

Hönninger, G., von Friedeburg, C., and Platt, U.: Multi axis differential optical absorption spectroscopy (MAX-DOAS), Atmos. Chem. Phys., 4, 231–254, doi:10.5194/acp-4-231-2004, 2004.

Huijnen, V., Eskes, H. J., Poupkou, A., Elbern, H., Boersma, K. F., Foret, G., Sofiev, M., Valdebenito, A., Flemming, J., Stein, O., Gross, A., Robertson, L., D'Isidoro, M., Kioutsioukis, I., Friese, E., Amstrup, B., Bergstrom, R., Strunk, A., Vira, J., Zyryanov, D., Maurizi, A., Melas, D., Peuch, V.-H., and Zerefos, C.: Comparison of OMI NO_2 tropospheric columns with an ensemble of global and European regional air quality models, Atmos. Chem. Phys., 10, 3273–3296, doi:10.5194/acp-10-3273-2010, 2010.

Irie, H., Kanaya, Y., Akimoto, H., Tanimoto, H., Wang, Z., Gleason, J. F., and Bucsela, E. J.: Validation of OMI tropospheric NO_2 column data using MAX-DOAS measurements deep inside the North China Plain in June 2006: Mount Tai Experiment 2006, Atmos. Chem. Phys., 8, 6577–6586, doi:10.5194/acp-8-6577-2008, 2008a.

ACPD
14, 2883–2934, 2014

Irie, H., Kanaya, Y., Akimoto, H., Iwabuchi, H., Shimizu, A., and Aoki, K.: First retrieval of tropospheric aerosol profiles using MAX-DOAS and comparison with lidar and sky radiometer measurements, Atmos. Chem. Phys., 8, 341–350, doi:10.5194/acp-8-341-2008, 2008b.

Irie, H., Kanaya, Y., Takashima, H., Gleason, J. F., and Wang, Z.: Characterization of OMI tropospheric NO_2 measurements in East Asia based on a robust validation comparison, SOLA, 5, 117–120, 2009a.

Irie, H., Kanaya, Y., Akimoto, H., Iwabuchi, H., Shimizu, A., and Aoki, K.: Dual-wavelength aerosol vertical profile measurements by MAX-DOAS at Tsukuba, Japan, Atmos. Chem. Phys., 9, 2741–2749, doi:10.5194/acp-9-2741-2009, 2009b.

Irie, H., Takashima, H., Kanaya, Y., Boersma, K. F., Gast, L., Wittrock, F., Brunner, D., Zhou, Y., and Van Roozendael, M.: Eight-component retrievals from ground-based MAX-DOAS observations, Atmos. Meas. Tech., 4, 1027–1044, doi:10.5194/amt-4-1027-2011, 2011.

Irie, H., Boersma, K. F., Kanaya, Y., Takashima, H., Pan, X., and Wang, Z. F.: Quantitative bias estimates for tropospheric NO_2 columns retrieved from SCIAMACHY, OMI, and GOME-2 using a common standard for East Asia, Atmos. Meas. Tech., 5, 2403–2411, doi:10.5194/amt-5-2403-2012, 2012.

Iwabuchi, H.: Efficient Monte Carlo methods for radiative transfer modeling, J. Atmos. Sci., 63, 9, 2324–2339, 2006.

Kanaya, Y., Sadanaga, Y., Nakamura, K., and Akimoto, H.: Behavior of OH and HO_2 radicals during the Observations at a Remote Island of Okinawa (ORION99) field campaign: 1. Observation using a laser-induced fluorescence instrument, J. Geophys. Res., 106, 24197–24208, doi:10.1029/2000JD000178, 2001.

Kannari, A., Tonooka, Y., Baba, T., Murano, K.: Development of multiple-species 1 km × 1 km resolution hourly basis emissions inventory for Japan, Atmos. Environ., 41, 3428–3439, 2007.

Kondo, Y., Morino, Y., Fukuda, M., Kanaya, Y., Miyazaki, Y., Takegawa, N., Tanimoto, H., McKenzie, R., Johnston, P., Blake, D. R., Murayama, T., and Koike, M.: Formation and transport of oxidized reactive nitrogen, ozone, and secondary organic aerosol in Tokyo, J. Geophys. Res., 113, D21310, doi:10.1029/2008JD010134, 2008.

Lamsal, L. N., Martin, R. V., van Donkelaar, A., Celarier, E. A., Bucsela, E. J., Boersma, K. F., Dirksen, R., Luo, C., and Wang, Y.: Indirect validation of tropospheric nitrogen dioxide retrieved from the OMI satellite instrument: insight into the seasonal variation of nitrogen ox-

ACPD
14, 2883–2934, 2014

ides at northern midlatitudes, J. Geophys. Res., 115, D05302, doi:10.1029/2009JD013351, 2010.

Lin, J.-T., Martin, R. V., Boersma, K. F., Sneep, M., Stammes, P., Spurr, R., Wang, P., Van Roozendael, M., Clémer, K., and Irie, H.: Retrieving tropospheric nitrogen dioxide over China from the Ozone Monitoring Instrument: effects of aerosols, surface reflectance anisotropy and vertical profile of nitrogen dioxide, Atmos. Chem. Phys. Discuss., 13, 21203–21257, doi:10.5194/acpd-13-21203-2013, 2013.

Ma, J. Z., Beirle, S., Jin, J. L., Shaiganfar, R., Yan, P., and Wagner, T.: Tropospheric NO_2 vertical column densities over Beijing: results of the first three years of ground-based MAX-DOAS measurements (2008–2011) and satellite validation, Atmos. Chem. Phys., 13, 1547–1567, doi:10.5194/acp-13-1547-2013, 2013.

Martin, R. V., Sioris, C. E., Chance, K., Ryerson, T. B., Bertram, T. H., Wooldridge, P. J., Cohen, R. C., Neuman, J. A., Swanson, A., and Flocke, F. M.: Evaluation of space-based constraints on global nitrogen oxide emissions with regional aircraft measurements over and downwind of eastern North America, J. Geophys. Res., 111, D15308, doi:10.1029/2005JD006680, 2006.

Peters, E., Wittrock, F., Großmann, K., Frieß, U., Richter, A., and Burrows, J. P.: Formaldehyde and nitrogen dioxide over the remote western Pacific Ocean: SCIAMACHY and GOME-2 validation using ship-based MAX-DOAS observations, Atmos. Chem. Phys., 12, 11179–11197, doi:10.5194/acp-12-11179-2012, 2012.

Piters, A. J. M., Boersma, K. F., Kroon, M., Hains, J. C., Van Roozendael, M., Wittrock, F., Abuhassan, N., Adams, C., Akrami, M., Allaart, M. A. F., Apituley, A., Beirle, S., Bergwerff, J. B., Berkhout, A. J. C., Brunner, D., Cede, A., Chong, J., Clémer, K., Fayt, C., Frieß, U., Gast, L. F. L., Gil-Ojeda, M., Goutail, F., Graves, R., Griesfeller, A., Großmann, K., Hemerijckx, G., Hendrick, F., Henzing, B., Herman, J., Hermans, C., Hoexum, M., van der Hoff, G. R., Irie, H., Johnston, P. V., Kanaya, Y., Kim, Y. J., Klein Baltink, H., Kreher, K., de Leeuw, G., Leigh, R., Merlaud, A., Moerman, M. M., Monks, P. S., Mount, G. H., Navarro-Comas, M., Oetjen, H., Pazmino, A., Perez-Camacho, M., Peters, E., du Piesanie, A., Pinardi, G., Puentedura, O., Richter, A., Roscoe, H. K., Schönhardt, A., Schwarzenbach, B., Shaiganfar, R., Sluis, W., Spinei, E., Stolk, A. P., Strong, K., Swart, D. P. J., Takashima, H., Vlemmix, T., Vrekoussis, M., Wagner, T., Whyte, C., Wilson, K. M., Yela, M., Yilmaz, S., Zieger, P., and Zhou, Y.: The Cabauw Intercomparison campaign for Nitrogen Dioxide measuring In-

ACPD
14, 2883–2934, 2014

struments (CINDI): design, execution, and early results, Atmos. Meas. Tech., 5, 457–485, doi:10.5194/amt-5-457-2012, 2012.
Platt, U.: Differential optical absorption spectroscopy (DOAS), Chem. Anal. Series, 127, 27–83, 1994.
Richter, A., Burrows, J. P., Nuss, H., Granier, C., and Niemeier, U.: Increase in tropospheric nitrogen dioxide over China observed from space, Nature, 437, 129–132, 2005.
Rodgers, C. D.: Inverse methods for atmospheric sounding: theory and practice, Ser. Atmos. Oceanic Planet. Phys., 2, edited by: Taylor, F. W., World Sci., Hackensack, NJ, 2000.
Roscoe, H. K., Van Roozendael, M., Fayt, C., du Piesanie, A., Abuhassan, N., Adams, C., Akrami, M., Cede, A., Chong, J., Clémer, K., Friess, U., Gil Ojeda, M., Goutail, F., Graves, R., Griesfeller, A., Grossmann, K., Hemerijckx, G., Hendrick, F., Herman, J., Hermans, C., Irie, H., Johnston, P. V., Kanaya, Y., Kreher, K., Leigh, R., Merlaud, A., Mount, G. H., Navarro, M., Oetjen, H., Pazmino, A., Perez-Camacho, M., Peters, E., Pinardi, G., Puentedura, O., Richter, A., Schönhardt, A., Shaiganfar, R., Spinei, E., Strong, K., Takashima, H., Vlemmix, T., Vrekoussis, M., Wagner, T., Wittrock, F., Yela, M., Yilmaz, S., Boersma, F., Hains, J., Kroon, M., Piters, A., and Kim, Y. J.: Intercomparison of slant column measurements of NO_2 and O_4 by MAX-DOAS and zenith-sky UV and visible spectrometers, Atmos. Meas. Tech., 3, 1629–1646, doi:10.5194/amt-3-1629-2010, 2010.
Rothman, L. S., Barbe, A., Chris Benner, D., and Hitran-Team.: The HITRAN molecular spectroscopic database: edition of 2000 including updates through 2001, J. Quant. Spectrosc. Ra., 82, 5–44, 2003.
Shaiganfar, R., Beirle, S., Sharma, M., Chauhan, A., Singh, R. P., and Wagner, T.: Estimation of NO_x emissions from Delhi using Car MAX-DOAS observations and comparison with OMI satellite data, Atmos. Chem. Phys., 11, 10871–10887, doi:10.5194/acp-11-10871-2011, 2011.
Sinreich, R., Frieß, U., Wagner, T., and Platt, U.: Multi axis differential optical absorption spectroscopy (MAX-DOAS) of gas and aerosol distributions, Faraday Discuss., 130, 153–164, doi:10.1039/b419274p, 2005.
Sudo, K., Takahashi, M., Kurokawa, J., and Akimoto, H.: CHASER: A global chemical model of the troposphere 1. Model description, J. Geophys. Res., 107, 4339, doi:10.1029/2001JD001113, 2002.

ACPD
14, 2883–2934, 2014

Takami, A., Miyoshi, T., Shimono, A., Kaneyasu, N., Kato, S., Kajii, Y., and Hatakeyama, S.: Transport of anthropogenic aerosols from Asia and subsequent chemical transformation, J. Geophys. Res., 112, D22S31, doi:10.1029/2006JD008120, 2007.

Takashima, H., Irie, H., Kanaya, Y., Shimizu, A., Aoki, K., and Akimotom, H.: Atmospheric aerosol variations at Okinawa Island in Japan observed by MAX-DOAS using a new cloud-screening method, J. Geophys. Res., 114, D18213, doi:10.1029/2009JD011939, 2009.

Takashima, H., Irie, H., Kanaya, Y., and Akimoto, H.: Enhanced NO_2 at Okinawa Island, Japan caused by rapid air mass transport from China as observed by MAX-DOAS, Atmos. Environ., 45, 2593–2597, 2011.

Takashima, H., Irie, H., Kanaya, Y., and Syamsudin, F.: NO_2 observations over the western Pacific and Indian Ocean by MAX-DOAS on *Kaiyo*, a Japanese research vessel, Atmos. Meas. Tech., 5, 2351–2360, doi:10.5194/amt-5-2351-2012, 2012.

Theys, N., Van Roozendael, M., Hendrick, F., Fayt, C., Hermans, C., Baray, J.-L., Goutail, F., Pommereau, J.-P., and De Mazière, M.: Retrieval of stratospheric and tropospheric BrO columns from multi-axis DOAS measurements at Reunion Island (21° S, 56° E), Atmos. Chem. Phys., 7, 4733–4749, doi:10.5194/acp-7-4733-2007, 2007.

Valks, P., Pinardi, G., Richter, A., Lambert, J.-C., Hao, N., Loyola, D., Van Roozendael, M., and Emmadi, S.: Operational total and tropospheric NO_2 column retrieval for GOME-2, Atmos. Meas. Tech., 4, 1491–1514, doi:10.5194/amt-4-1491-2011, 2011.

Vandaele, A. C., Hermans, C., Simon, P. C., Van Roozendael, M., Guilmot, J. M., Carleer, M., and Colin, R.: Fourier transform measurement of NO_2 absorption cross-section in the visible range at room temperature, J. Atmos. Chem., 25, 289–305, 1996.

van der A, R. J., Eskes, H. J., Boersma, K. F., van Noije, T. P. C., Van Roozendael, M., De Smedt, I., Peters, D. H. M. U., and Meijer, E. W.: Trends, seasonal variability and dominant NO_x source derived from a ten year record of NO_2 measured from space, J. Geophys. Res., 113, D04302, doi:10.1029/2007JD009021, 2008.

Wagner, T., Burrows, J. P., Deutschmann, T., Dix, B., von Friedeburg, C., Frieß, U., Hendrick, F., Heue, K.-P., Irie, H., Iwabuchi, H., Kanaya, Y., Keller, J., McLinden, C. A., Oetjen, H., Palazzi, E., Petritoli, A., Platt, U., Postylyakov, O., Pukite, J., Richter, A., van Roozendael, M., Rozanov, A., Rozanov, V., Sinreich, R., Sanghavi, S., and Wittrock, F.: Comparison of box-air-mass-factors and radiances for Multiple-Axis Differential Optical Absorption Spectroscopy (MAX-DOAS) geometries calculated from different UV/visible radiative transfer models, Atmos. Chem. Phys., 7, 1809–1833, doi:10.5194/acp-7-1809-2007, 2007.

ACPD
14, 2883–2934, 2014

Watanabe, S., Takemura, T., Sudo, K., Yokohata, T., and Kawase, H.: Anthropogenic changes in the surface all-sky UV-B radiation through 1850–2005 simulated by an Earth system model, Atmos. Chem. Phys., 12, 5249–5257, doi:10.5194/acp-12-5249-2012, 2012.

Wenig, M. O., Cede, A. M., Bucsela, E. J., Celarier, E. A., Boersma, K. F., Veefkind, J. P., Brinksma, E. J., Gleason, J. F., and Herman, J. R.: Validation of OMI tropospheric NO_2 column densities using direct-Sun mode Brewer measurements at NASA Goddard Space Flight Center, J. Geophys. Res., 113, D16S45, doi:10.1029/2007JD008988, 2008.

Wittrock, F., Oetjen, H., Richter, A., Fietkau, S., Medeke, T., Rozanov, A., and Burrows, J. P.: MAX-DOAS measurements of atmospheric trace gases in Ny-Ålesund – Radiative transfer studies and their application, Atmos. Chem. Phys., 4, 955–966, doi:10.5194/acp-4-955-2004, 2004.

Yurganov, L., McMillan, W., Grechko, E., and Dzhola, A.: Analysis of global and regional CO burdens measured from space between 2000 and 2009 and validated by ground-based solar tracking spectrometers, Atmos. Chem. Phys., 10, 3479–3494, doi:10.5194/acp-10-3479-2010, 2010.

Zhang, Q., Streets, D. G., Carmichael, G. R., He, K. B., Huo, H., Kannari, A., Klimont, Z., Park, I. S., Reddy, S., Fu, J. S., Chen, D., Duan, L., Lei, Y., Wang, L. T., and Yao, Z. L.: Asian emissions in 2006 for the NASA INTEX-B mission, Atmos. Chem. Phys., 9, 5131–5153, doi:10.5194/acp-9-5131-2009, 2009.

Zhou, Y., Brunner, D., Boersma, K. F., Dirksen, R., and Wang, P.: An improved tropospheric NO_2 retrieval for OMI observations in the vicinity of mountainous terrain, Atmos. Meas. Tech., 2, 401–416, doi:10.5194/amt-2-401-2009, 2009.

ACPD
14, 2883–2934, 2014

Table 1. List of locations for MAX-DOAS observations.

Location	Latitude (°N)	Longitude (°E)	Surface Elevation (m)	Instrument Elevation (m)	Azimuth angle (°, from North, clockwise)	Instruments and used periods	N (NO_2 retrievals)
Yokosuka	35.32	139.65	0	10	+37	#1, Apr 2007–Dec 2012	26 554
Cape Hedo	26.87	128.25	0	68	−14	#1, Mar 2007–Dec 2012	18 367
Gwangju	35.23	126.84	30	43	+44	#1, Feb 2008–Jun 2009 #2, Nov 2009–Aug 2010 #3, May 2011–Dec 2012	11 349
Hefei	31.91	117.16	30	51	+22	#1, Mar 2008–Oct 2009 #2, Nov 2009–Dec 2012	5,324
Zvenigorod	55.70	36.78	186	208	−32	#1, Oct 2008–Dec 2012	8,948
Tomsk	56.48	85.05	160	188	0	#1, Jan 2009–Dec 2012	–
Fukue	32.75	128.68	80	83	+30	#1, Mar 2009–Apr 2009 #2, Apr 2009–Mar 2012 #3, Mar 2012–Dec 2012	10 385
TOTAL							**80 927**

ACPD
14, 2883–2934, 2014

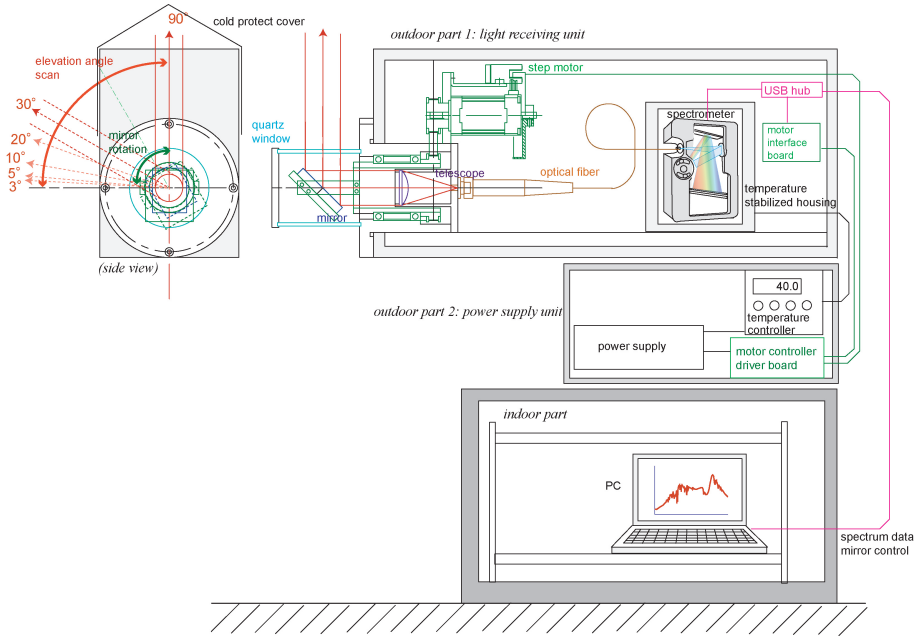

Fig. 1. Schematic diagram of MAX-DOAS instrument used at Zvenigorod.

ACPD
14, 2883–2934, 2014

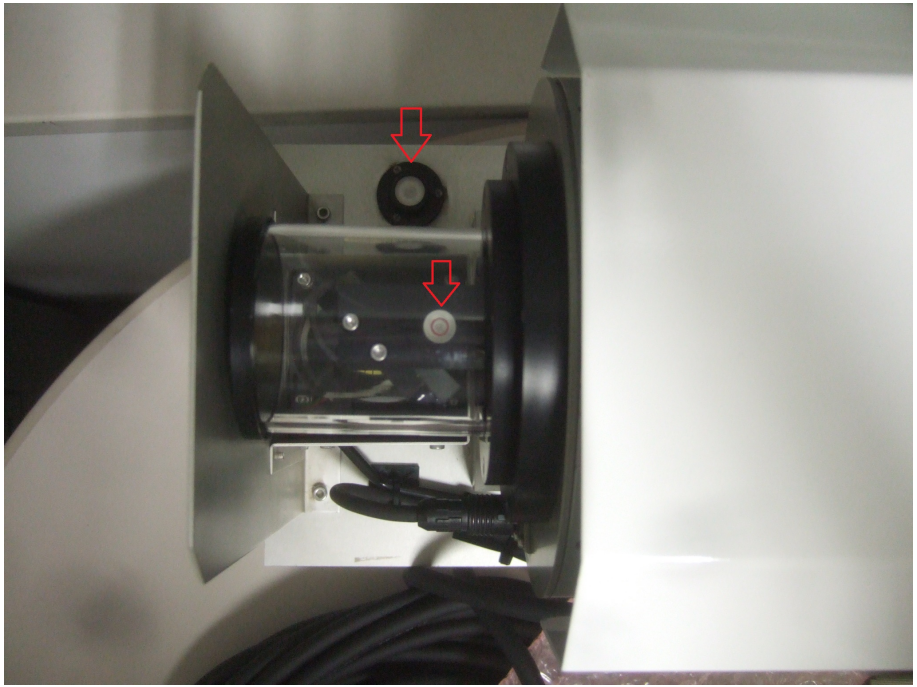

Fig. 2. Two horizontal levels embedded in the base plate (upper arrow) and in a plate holding the reflecting mirror (lower arrow) were used to adjust the zero angle of the reflecting mirror.

ACPD
14, 2883–2934, 2014

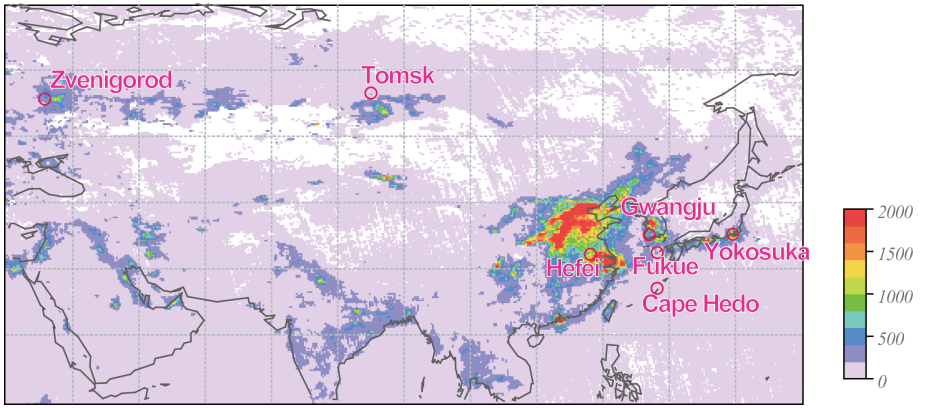

Fig. 3. Locations of our MAX-DOAS observations. The background contour is based on the TropoNO_2VCD (10^{13} molecules cm^{-2}) observed by OMI (DOMINO ver. 2.0).

ACPD
14, 2883–2934, 2014

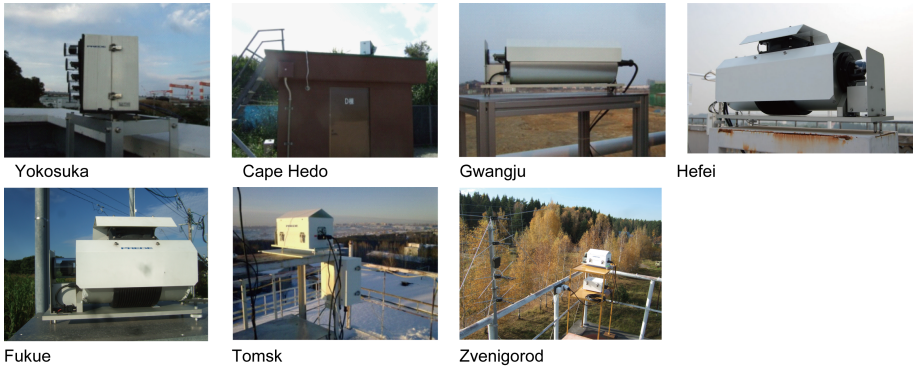

Fig. 4. Light-receiving parts of MAX-DOAS instruments located at the seven sites.

ACPD
14, 2883–2934, 2014

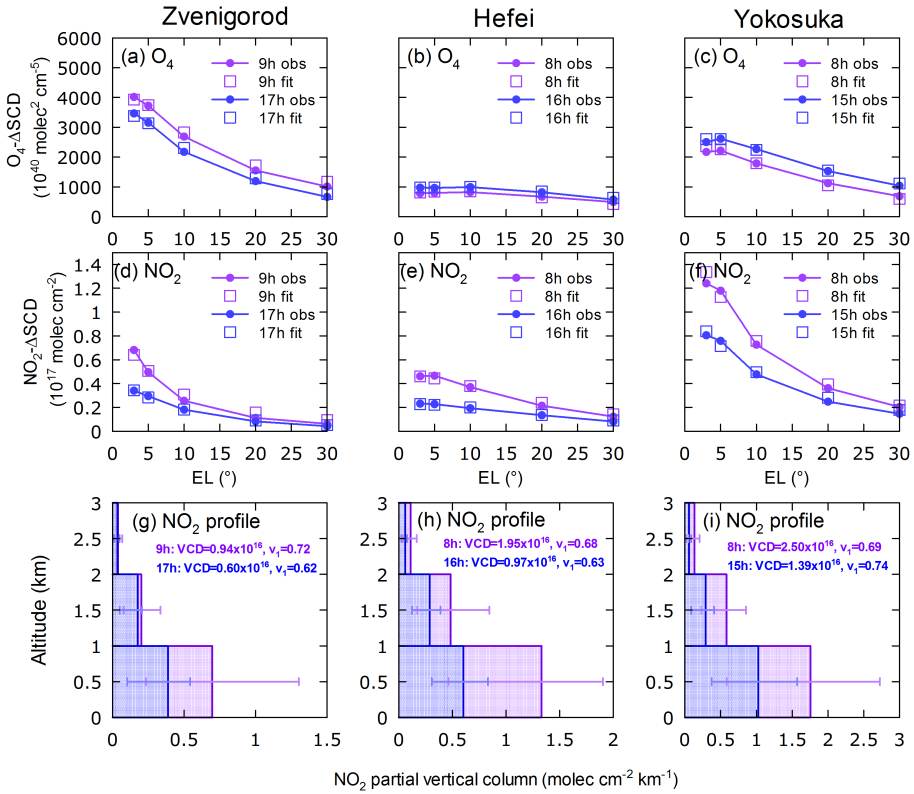

Fig. 5. (a–f) Observed and fitted $O_4\Delta$SCDs and $NO_2\Delta$SCDs, and **(g–i)** optimally estimated NO_2 vertical profiles averaged over each 1 h period in the morning and afternoon at Zvenigorod, Hefei, and Yokosuka sites, respectively. For **(g–i)**, error bars represent 1σ range of individual profiles included in the hours.

ACPD
14, 2883–2934, 2014

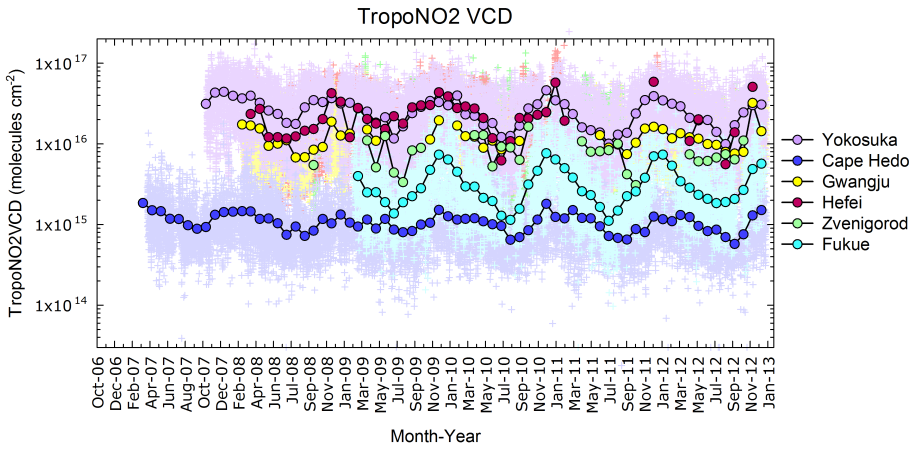

Fig. 6. Time series of all individual observations of TropoNO2VCD (plus signs, 30 min time resolution) and their monthly averages (circles).

ACPD
14, 2883–2934, 2014

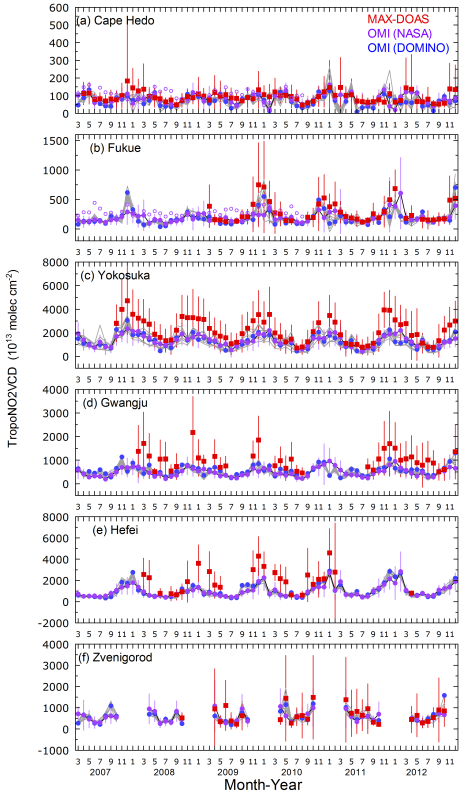

Fig. 7. Time series of monthly averages of MAX-DOAS (red) and satellite observations of TropoNO2VCD. The satellite observations are derived using NASA (ver. 2.1, purple) and DOMINO (ver. 2.0, blue) algorithms. Open purple circles in **(a)** and **(b)** represent data from older products (NASA ver. 1). Error bars of MAX-DOAS represent 1σ ranges of included data. Error bars of OMI with NASA ver. 2.1 algorithm were calculated from 1σ ranges of daily data included in the month. Gray lines represent OMI data using DOMINO ver. 2.0 algorithm at the eight grids (0.125° × 0.125°) adjacent to the grid nearest the site (blue circles).

ACPD
14, 2883–2934, 2014

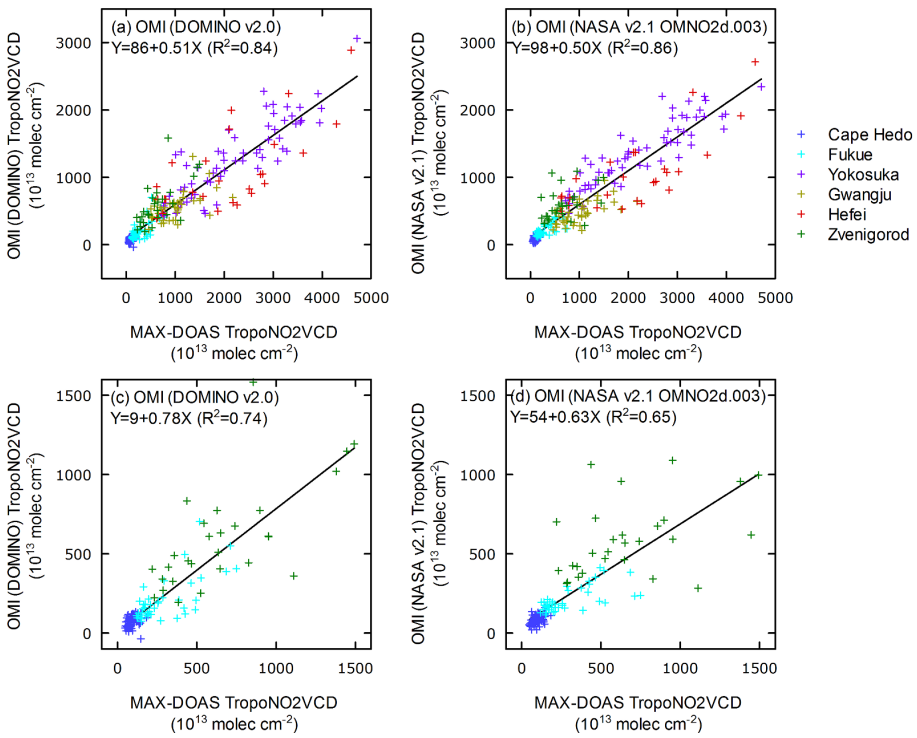

Fig. 8. Scatterplots between monthly averages of TropoNO2VCD derived from OMI and MAX-DOAS for **(a)** and **(b)** all sites, and for **(c)** and **(d)** three rural/remote sites, using DOMINO ver. 2.0 for **(a)** and **(c)**, and NASA ver. 2.1 for **(b)** and **(d)**.

ACPD
14, 2883–2934, 2014

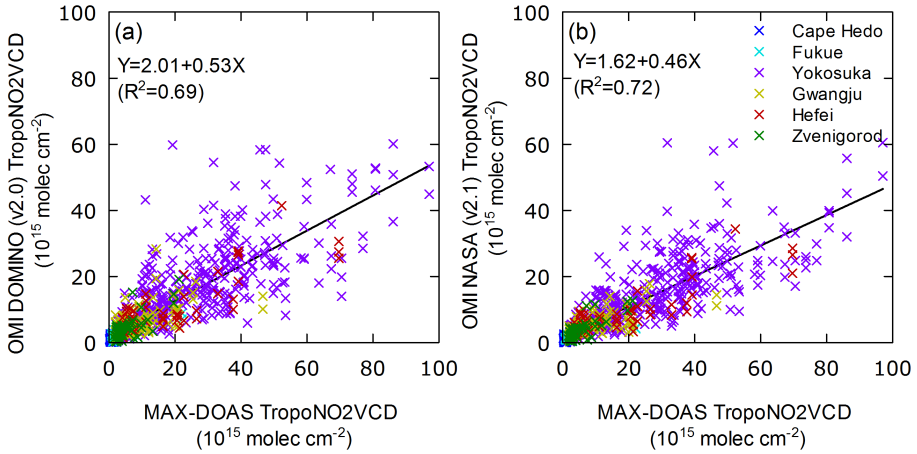

Fig. 9. Similar to Fig. 8 but for pixel-based comparisons with strict coincidence criteria (horizontal displacement < 0.15°, time difference < 15 min), and cloud screening (cloud fraction < 10 %); DOMINO (ver. 2.0) and NASA (ver. 2.1) were used for **(a)** and **(b)**, respectively.

ACPD
14, 2883–2934, 2014

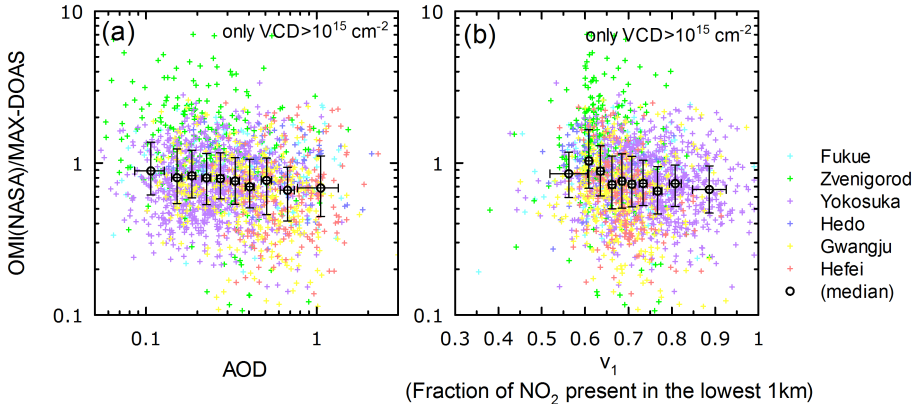

Fig. 10. OMI(NASA)/MAX-DOAS ratios for TropoNO2VCD were plotted against **(a)** AOD at 476 nm, observed with MAX-DOAS and **(b)** v_1, a retrieved parameter defining the fraction of NO_2 present in the lowest 1 km. Black circles and error bars represent the median ratios and 1σ ranges for the 10 bins sorted by AOD and v_1, respectively.

ACPD
14, 2883–2934, 2014

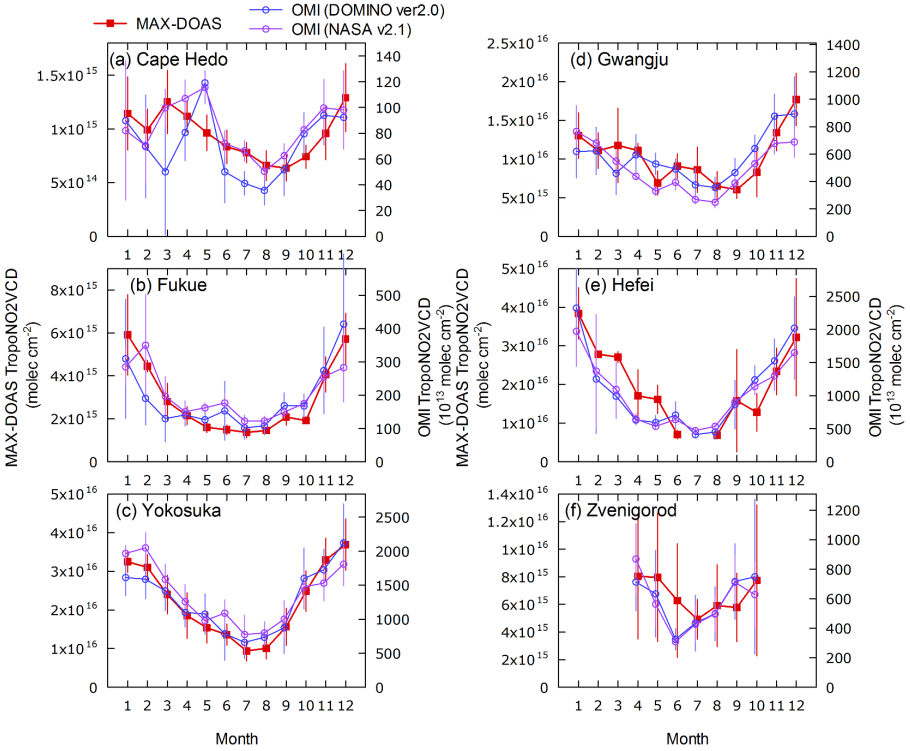

Fig. 11. Seasonality comparisons for TropoNO2VCD values derived from MAX-DOAS and satellite observations. MAX-DOAS data from the hours of satellite observations were used. The error bars represent variability in the monthly average TropoNO2VCD values over the studied years.

ACPD
14, 2883–2934, 2014

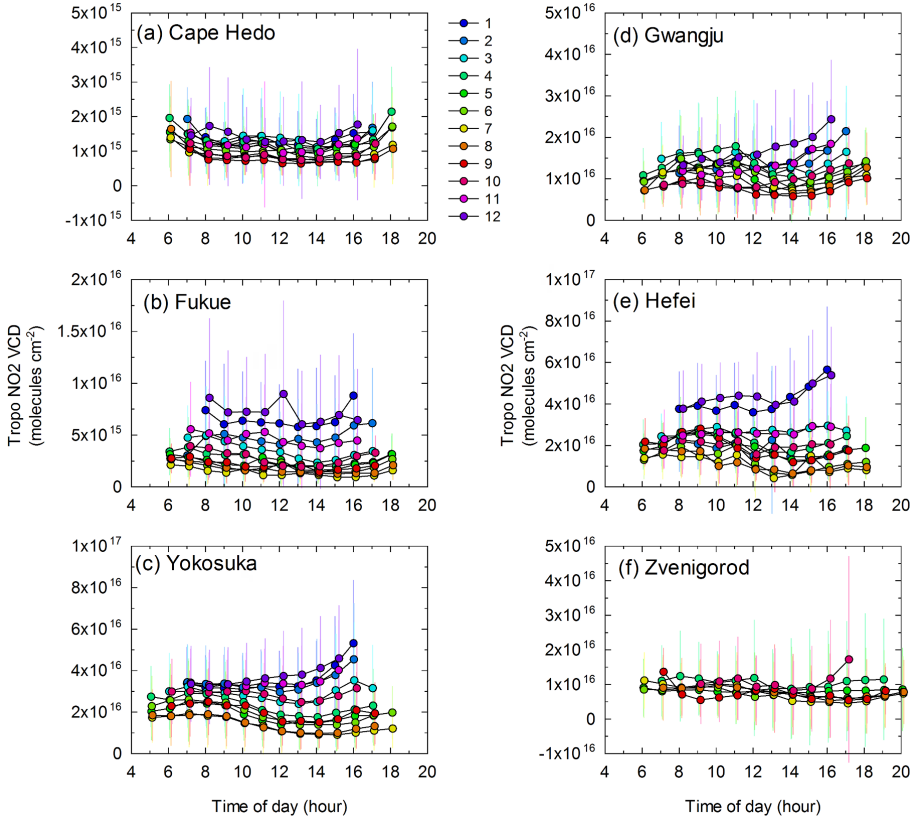

Fig. 12. Average diurnal variations in TropoNO2VCD for each month (differently colored). Error bars represent the 1σ range of the included data.

ACPD
14, 2883–2934, 2014

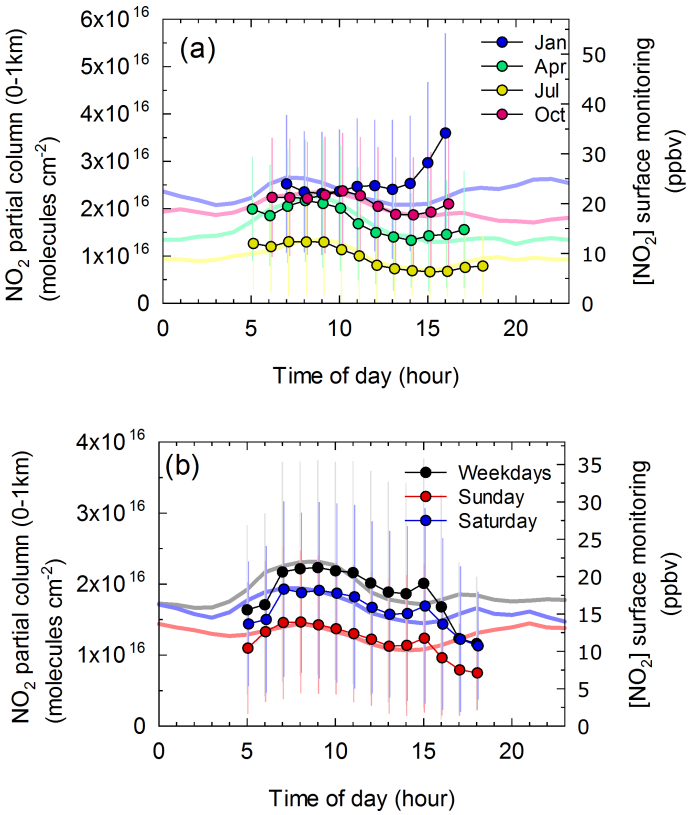

Fig. 13. Comparison of average diurnal cycles of NO_2 observed by MAX-DOAS at Yokosuka (partial columns in the lowest 1 km layer, colored circles) and by surface monitoring at Nagahama (near Yokosuka, pale colored lines) for **(a)** four selected months (January, April, July, and October) and for **(b)** weekdays and weekends. Error bars represent the 1σ range of the included data (MAX-DOAS).

ACPD
14, 2883–2934, 2014

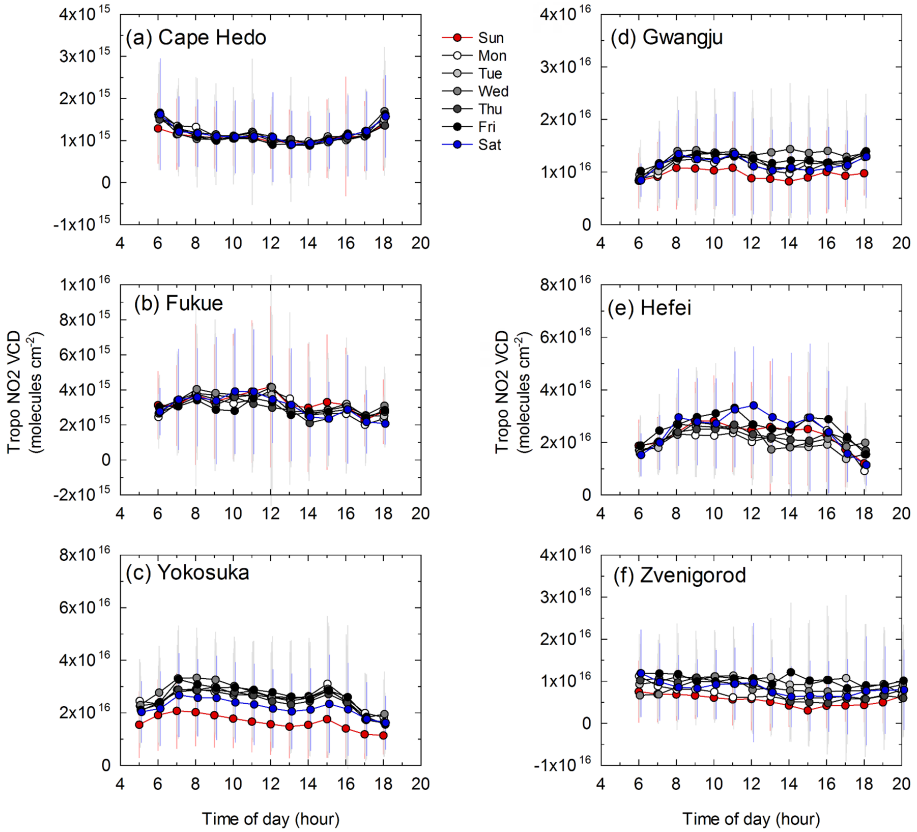

Fig. 14. Diurnal variations in TropoNO2VCD separately averaged for days of the week. Error bars represent the 1σ range of the included data.

ACPD
14, 2883–2934, 2014

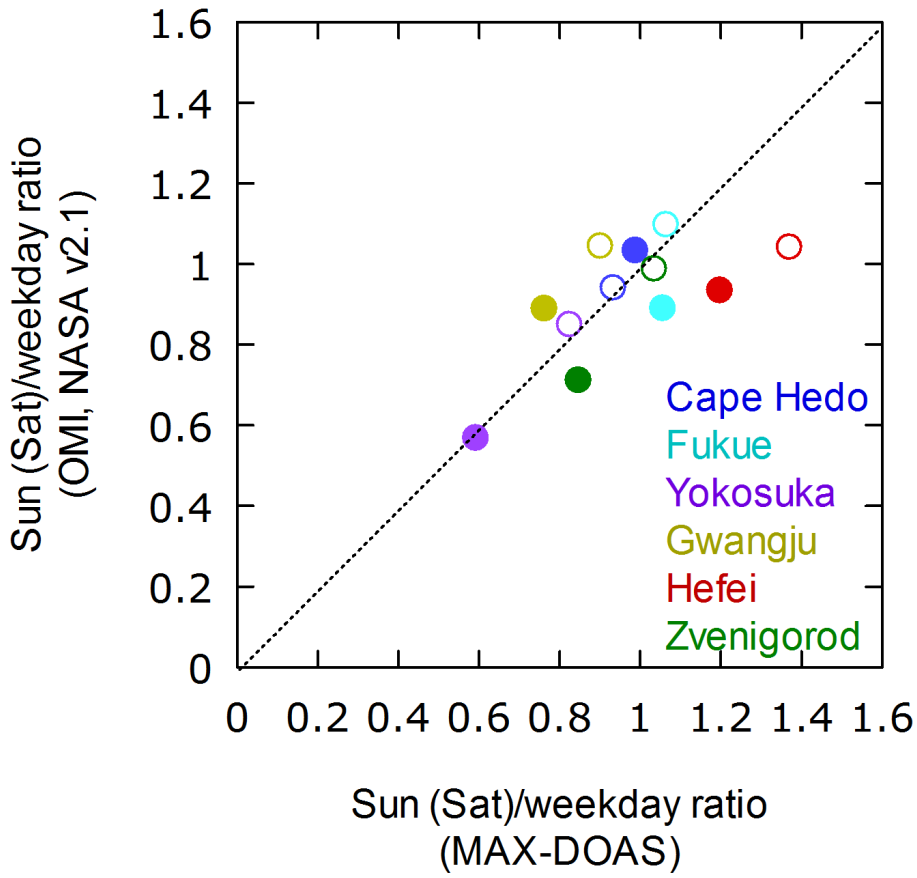

Fig. 15. Weekend reduction ratios for TropoNO2VCD derived from MAX-DOAS and OMI (using NASA ver. 2.1 algorithm). Open and closed symbol represent Saturdays and Sundays, respectively.

ACPD
14, 2883–2934, 2014

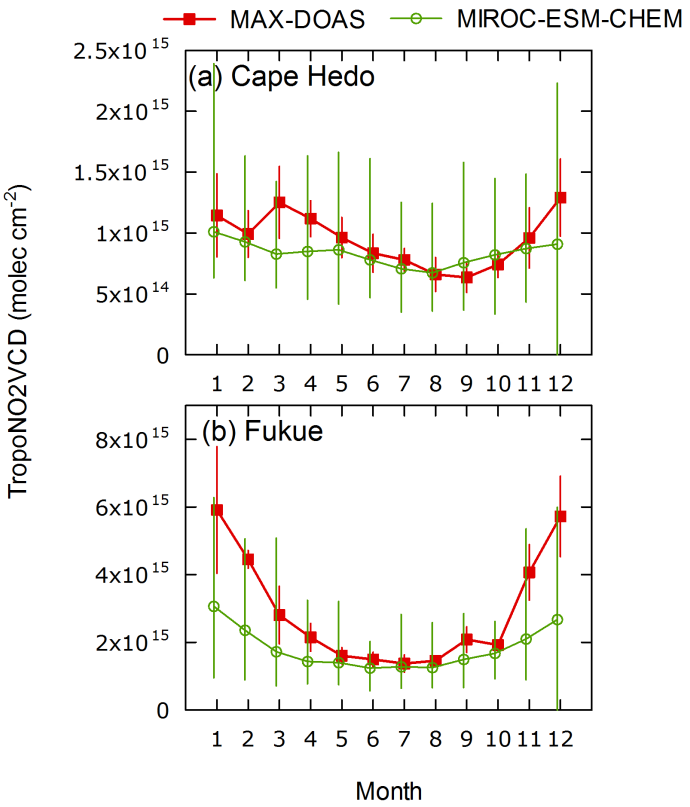

Fig. 16. Comparisons of average seasonal variations in TropoNO2VCD derived from MAX-DOAS observations and model simulations (MIROC-ESM-CHEM). Data from the hours of satellite observations (OMI) are used. Error bars for MAX-DOAS represent variations in the monthly averages over the studied years, whereas those for model simulations represent the full ranges of hourly averages included in each hour.

ACPD
14, 2883–2934, 2014

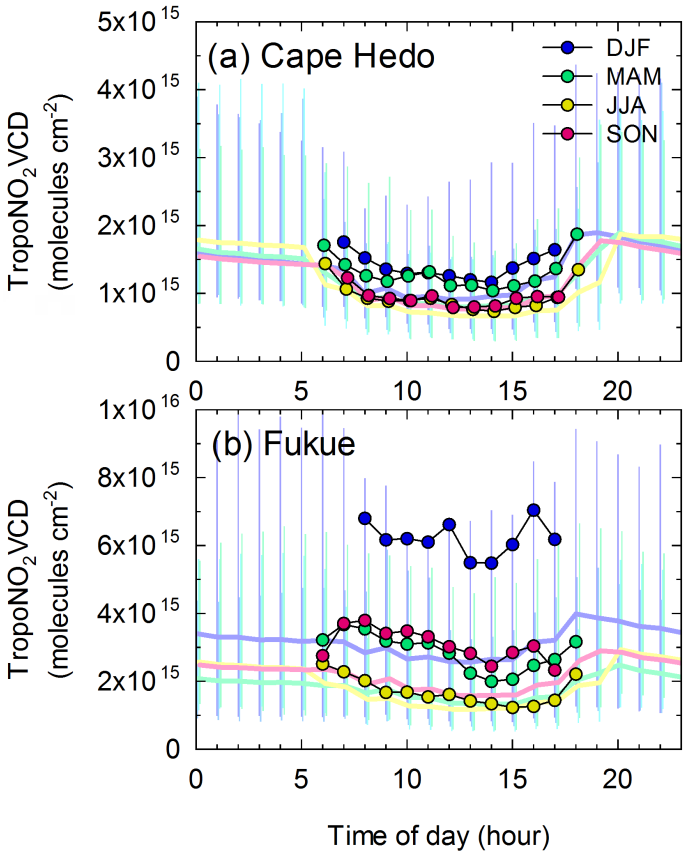

Fig. 17. Comparisons of average diurnal variations in TropoNO2VCD derived from MAX-DOAS observations (colored circles) and MIROC-ESM-CHEM model simulations (pale colored lines) for four seasons. Error bars for model simulations represent full ranges of hourly averages included in each hour.

ACPD
14, 2883–2934, 2014